Journal of Natural Remedies
DOI: 10.18311/jnr/2026/54026

INFORMATICS JOURNALS
Research Article
eISSN: 2320-3358 | Vol 26(2), 2026 | pp. 483-506

Development and Evaluation of Topical Nano Formulation of Leaf of *Adina cordifolia* for Wound Healing Activity

Rakesh Surappa Anjaneya[1*] and Guno Sindhu Chakraborty[2]

[1]Faculty of Pharmacy, Parul Institute of Pharmacy and Research, Parul University, Vadodara – 391760, Gujarat, India; rakesh.sagmipsr@gmail.com

[2]Department of Pharmacognosy, Parul Institute of Pharmacy and Research, Parul University, Vadodara – 391760, Gujarat, India

Abstract

Background: Chronic and acute wounds remain a significant clinical challenge due to delayed healing, infection risk, and limitations of conventional topical therapies. The integration of medicinal plant-derived bioactives with nanotechnology offers a promising strategy to enhance wound repair and therapeutic outcomes. **Aim:** This study aimed to develop and evaluate a novel topical nano-hydrogel formulation containing *Adina cordifolia* leaf extract-mediated Copper Oxide (CuO) nanoparticles for enhanced wound healing activity. **Methods:** CuO nanoparticles were synthesised using a green synthesis approach employing *A. cordifolia* leaf extract and characterised by UV-visible spectroscopy, X-ray Diffraction (XRD), particle size analysis, and zeta potential measurement. The nanoparticles were incorporated into a Carbopol 934-based hydrogel. Formulation optimisation was performed using a central composite design, generating thirteen formulations (HGL1-HGL13). The optimised formulation was evaluated for *in vitro* drug release kinetics, drug-excipient compatibility, stability, and model validation. *In vivo* wound healing efficacy was assessed in Wistar rats by monitoring wound contraction and epithelialisation over 15 days. **Results:** The synthesised CuO nanoparticles showed a mean particle size of 365.3 ± 118.2 nm and a zeta potential of −26.6 mV, indicating good stability. UV-visible spectroscopy (λmax 264 nm) and XRD peaks at 35° and 38° confirmed nanoparticle formation and crystalline nature. Among all formulations, HGL7 exhibited optimal performance with 81% cumulative drug release over 12 h following zero-order kinetics ($R^2 = 1$). Compatibility and validation studies confirmed formulation stability and high predictability (bias < ±1%). *In vivo* studies demonstrated significantly enhanced wound contraction and epithelialisation in nano-hydrogel-treated animals compared to conventional treatment. **Conclusion:** The developed *A. cordifolia*-based CuO nano-hydrogel represents a stable, reproducible, and effective topical formulation that significantly enhances wound healing. This study highlights the potential of combining traditional herbal medicine with nanotechnology for advanced wound care and future clinical and commercial applications.

Major Findings: The study developed a stable nano-hydrogel using green-synthesised CuO nanoparticles from *A. cordifolia*, showing optimal properties and controlled drug release. The optimised formulation (HGL7) significantly accelerated wound contraction and epithelialisation *in vivo*. These findings demonstrate its strong potential as an effective advanced wound care treatment.

Keywords: *A. cordifolia* Leaf, Controlled Release, Copper Oxide Nanoparticles, Green Synthesis, Hydrogel Formulation, Wound Healing

(Article Chronicle: Article Received on: 11.12.2025; Revised on: 20.01.2026; Accepted on: 29.01.2026)

1. Introduction

Wound healing remains a significant healthcare challenge, requiring effective therapeutic interventions that promote tissue regeneration while preventing complications. Traditional medicine and natural products have emerged as promising alternatives for wound management, offering reduced side effects

*Author for correspondence

and improved healing outcomes[1,2]. The integration of nanotechnology with traditional medicinal plants presents an innovative approach to enhance wound healing efficacy through improved delivery systems and therapeutic properties[3]. *Adina cordifolia (A. cordifolia)*, a traditional medicinal plant belonging to the family *Rubiaceae*, has garnered attention for its therapeutic potential. The development of nano formulation incorporating plant-derived compounds represents a significant advancement in wound healing therapeutics[4].

Recent studies have demonstrated that metal oxide nanoparticles, particularly Copper Oxide (CuO), exhibit remarkable wound healing properties when combined with natural extracts[5]. The current research landscape shows increasing interest in hydrogel-based delivery systems for wound healing applications. These formulations provide an optimal environment for wound healing by maintaining moisture balance, facilitating oxygen exchange, and ensuring controlled release of therapeutic agents[6,7]. The combination of nanoparticles with hydrogel matrices has shown enhanced efficacy in wound management, offering improved stability and bioavailability of active compounds[8,9].

The development of green-synthesised nanoparticles using plant extracts represents an eco-friendly and cost-effective approach. Recent studies have demonstrated that such biogenic nanoparticles exhibit enhanced therapeutic properties, including antimicrobial, anti-inflammatory, and wound-healing activities[4,10,11]. The incorporation of these nanoparticles into hydrogel formulations provides a promising platform for wound healing applications, addressing the limitations of conventional treatments while leveraging the benefits of both traditional medicine and modern pharmaceutical[10]. This research aims to develop and evaluate a novel topical nanoformulation combining CuO nanoparticles synthesised using *A. cordifolia* leaf extract with a hydrogel matrix, targeting enhanced wound healing efficacy through controlled release and improved tissue regeneration properties.

Herein, the hydrogel formulation was optimised using a central composite design with Carbopol 934 as the gelling agent. This resulted in thirteen formulations evaluated for physicochemical properties including pH, viscosity, and drug content uniformity[12,13]. *In vitro,* drug release studies were conducted using a modified diffusion apparatus over 12 hours in phosphate buffer, with release kinetics analysis demonstrating zero-order release for the optimised formulation. The wound healing efficacy was evaluated through *in vivo* studies using Wistar rats (160-180 g) with an excision wound model, monitoring wound contraction and epithelialisation over 16 days under standardised conditions[14,15].

This comprehensive research successfully developed a novel topical nano formulation combining green-synthesised CuO nanoparticles with *A. cordifolia* leaf extract in a hydrogel matrix, demonstrating controlled release properties, excellent stability, and enhanced wound healing efficacy compared to conventional treatments. The study established a promising platform for developing advanced wound healing formulations by integrating traditional medicine with modern pharmaceutical technology, supported by thorough physicochemical characterisation and *in vivo* validation studies.

2. Materials and Methods

2.1 Plant Materials

The materials used in this research work included leaves of *A. cordifolia*, which were collected, authenticated, and processed into a fine powder. Plant authentication number (DU-0256-23) Davangere University, Karnataka, India.

2.2 Chemicals and Equipment

Cupric nitrate trihydrate [$Cu(NO_3)_2 \cdot 3H_2O$] was used as the primary precursor for the synthesis of copper oxide nanoparticles (CuO-NPs). The synthesis process also utilised 95% ethanol for sonication purposes. For the preparation of the hydrogel formulation, the following materials were employed: The synthesised CuO-NPs, Carbopol 934 as a gelling agent, sodium hydroxide for pH adjustment, sodium benzoate as a preservative, glycerine as a humectant, and purified water as the vehicle. All chemicals and reagents used in this study were of analytical grade and obtained from reputable suppliers. The plant extract and nanoparticle synthesis were carried out using standard laboratory equipment, including a mechanical grinder, magnetic stirrer, and muffle furnace. Various analytical instruments were used for characterisation purposes, though specific

details of these instruments are not included in the materials section.

2.3 Preparation of Plant Extract

The preparation of the *A. cordifolia* leaf extract involved a straightforward process designed to efficiently extract bioactive compounds from the plant material. Initially, 2 g of dried *A. cordifolia* leaf powder was accurately weighed and transferred to a clean beaker. To this, 100 ml of sterile distilled water was added, creating a concentration of 2% w/v. The mixture was then subjected to agitation using a magnetic stirrer, operating at a speed between 450 to 500 rpm[16,17]. This stirring process was maintained for 15 min, which allowed sufficient time for the water to penetrate the plant material and extract the soluble compounds. The continuous agitation ensured thorough mixing and enhanced the extraction efficiency by increasing the contact between the solvent and the plant particles. After the stirring period, the resulting mixture was filtered to separate the liquid extract from the solid plant residue. The filtration process involved the use of filter paper or a suitable filtration apparatus to obtain a clear extract. The filtered extract was then collected and stored under appropriate conditions to maintain its integrity for subsequent use in nanoparticle synthesis and further experiments[18,19].

2.4 Synthesis of Copper Oxide Nanoparticles (CuO-NPs)

The synthesis of copper oxide nanoparticles (CuO-NPs) was accomplished using a modified solution combustion method[20]. This approach utilised the aqueous extract of *A. cordifolia* leaves as a reducing and stabilising agent. The process began with the preparation of the plant extract. 2 g of dried *A. cordifolia* leaf powder was dissolved in 100 ml of sterile distilled water. This mixture was then subjected to magnetic stirring at 450-500 rpm for 15 min to ensure thorough extraction of the bioactive compounds. For the nanoparticle synthesis, a stoichiometric amount of cupric nitrate trihydrate [$Cu(NO_3)_2 \cdot 3H_2O$] was dissolved in 5 ml of the prepared plant extract[10]. This solution was then carefully transferred to a preheated muffle furnace maintained at 350°C. The rapid heating induced a combustion reaction, resulting in the formation of CuO-NPs. Within a short period of 5-8 min, a blackish amorphous powder was observed, indicating the successful synthesis of CuO-NPs. This rapid formation is characteristic of the solution combustion method, where the plant extract acts as both a fuel and a reducing agent.

To optimise the synthesis conditions, the experiment was repeated using varying concentrations of the plant extract (5, 10, 15, 20, 25, and 30 ml) while keeping other parameters constant. This systematic approach allowed for the determination of the optimal extract concentration for nanoparticle formation. Upon completion of the synthesis, the CuO-NPs were collected and ground into a fine powder using a mortar and pestle. The resulting nanoparticles were then stored in airtight containers to prevent agglomeration and contamination, ensuring their stability for subsequent characterisation and application studies. This green synthesis method offers several advantages, including the use of environmentally friendly reagents, the simplicity of the process, and the potential for scalability. The use of *A. cordifolia* leaf extract not only facilitates the reduction of copper ions but may also contribute to the functionalisation of the nanoparticles with bioactive compounds, potentially enhancing their properties for various applications.

2.5 Characterisation of CuO Nanoparticles (CuO-NPs)

2.5.1 UV-Visible Spectroscopy

The optical properties of the synthesised nanoparticles were analysed using UV-Visible spectroscopy. Aqueous dispersions of the nanoparticles were prepared in deionised water and loaded into quartz cuvettes with a 1 cm optical path length[21]. Absorption spectra were recorded across 200-800 nm wavelengths at ambient temperature using a double-beam spectrophotometer. This technique helped identify characteristic surface plasmon resonance bands, confirming nanoparticle formation and stability.

2.5.2 Fourier-Transform Infrared (FTIR) Spectroscopy

Functional group analysis was conducted using FTIR spectroscopy (Bruker spectrometer). Samples were prepared via the KBr pellet method, where nanoparticles were homogenised with potassium bromide and compressed into transparent disks.

Spectra were acquired in the 4000-400 cm^{-1} range with a resolution of 4 cm^{-1}, averaging 32 scans to enhance signal-to-noise ratios[22]. This analysis revealed molecular interactions between phytochemicals in the plant extract and the nanoparticle surface, providing insights into stabilisation mechanisms.

2.5.3 Particle Size Distribution

Hydrodynamic diameter and polydispersity were determined via DLS using the same Zetasizer instrument. Suspensions were filtered through 0.45 µm membrane filters before analysis to remove aggregates[23]. Data interpretation employed cumulant analysis, reporting Z-average values and Polydispersity Indices (PDI) derived from intensity-weighted distributions of three technical replicates.

2.5.4 Zeta Potential Analysis

Surface charge and colloidal stability were assessed through zeta potential measurements using dynamic light scattering (Malvern Zetasizer Nano ZS)[24]. Nanoparticle suspensions were diluted in deionised water (pH 7.0) to achieve optimal scattering intensity and loaded into folded capillary cells. Measurements were conducted at 25°C with a 173° backscatter angle, averaging three consecutive readings per sample.

2.5.5 Scanning Electron Microscopy (SEM)

The surface morphology of the synthesised nanoparticles was investigated using SEM. Sample preparation involved uniformly dispersing the nanoparticle powder on carbon tape-mounted stubs, followed by gold sputter-coating (15 nm thickness) to minimise charging effects during imaging. Micrographs were acquired under high vacuum at accelerating voltages ranging from 5-20 kV, with magnifications spanning 5,000×-50,000× to resolve nanoscale surface features and agglomeration patterns[25].

2.5.6 Transmission Electron Microscopy (TEM)

Nanostructure characteristics were analysed using TEM operated at 200 kV. Samples were prepared by ultrasonically dispersing nanoparticles in ethanol and depositing the suspension onto carbon-coated copper grids (300 mesh). After air-drying, bright-field imaging was performed at multiple magnifications (50,000×-200,000×), complemented by Selected-Area Electron Diffraction (SAED) to confirm crystallinity and phase composition[26].

2.5.7 X-ray Diffraction (XRD)

Crystallographic properties were evaluated using XRD with Cu-Kα radiation (λ = 1.5406 Å). Scans were performed at 40 kV and 30 mA over a 2θ range of 20-80°, with a step size of 0.02° and a scan rate of 2° min^{-1}. Diffraction patterns were analysed to determine crystallite size, phase purity, and lattice parameters using Bragg's law and the Scherrer equation[27] Distinct peaks in the XRD profile confirmed the crystalline nature of the synthesised CuO nanoparticles.

2.6 Experimental Design and Optimisation of Formulation

2.6.1 Pre-formulation Study

Preformulation studies constitute the foundational phase in pharmaceutical development, involving a comprehensive evaluation of a drug substance's physicochemical properties to guide rational formulation design. This critical step facilitates the identification of inherent characteristics influencing drug stability, bioavailability, and compatibility with excipients. For the CuO nanoparticle (CuO-NP) hydrogel system, pre-formulation investigations focused on establishing critical quality attributes through material characterisation and compatibility assessments between the synthesised nanoparticles and polymeric components. These studies established essential parameters for developing an optimised topical delivery system with appropriate rheological properties, drug release kinetics, and physical stability.

2.6.2 Experimental Design for Formulation Optimisation

A Central Composite Design (CCD) coupled with response surface methodology (RSM) was employed to optimise the hydrogel formulation systematically[28,29]. The experimental design focused on two independent variables: Carbopol 934 concentration (% w/w) and homogenisation speed (rpm). Each variable was tested at five distinct levels, resulting in a total of 13 experimental runs, including six centre-point replicates for error estimation. The optimisation process targeted two dependent response variables: cumulative drug release over 12 h and entrapment efficiency (%). Design

Expert® 13.0.0 software was utilised to develop and analyse the experimental matrix. The CCD structure comprised 2^2 factorial points at ±1 level, four axial points at ±α level, and six centre-point replicates. This configuration allowed for the development of a quadratic model, enabling the evaluation of linear, interaction, and curvature effects between variables. The α value was set at 1.414 to maintain rotatability, ensuring consistent prediction variance across the design space. Response surface plots and ANOVA were employed to identify significant factors and establish optimal processing conditions through desirability function analysis, providing a comprehensive approach to formulation optimisation.

2.7 Preparation of CuO NPs-loaded Hydrogel

The hydrogel formulation was prepared using a sequential blending technique. Initially, CuO NPs (0.1% w/w) were uniformly dispersed in aliquots of 95% ethanol under continuous magnetic stirring (200 rpm, 25°C). Sodium benzoate (0.01% w/w) was incrementally titrated into the ethanolic dispersion to ensure homogeneity. The gel phase was prepared by hydrating Carbopol 934 (1% w/v) in purified water under mechanical stirring (500-1000 rpm, 30 min) at ambient temperature. Post-hydration, the pH of the gel phase was adjusted to 6.04 ± 0.2 using 0.1 M sodium hydroxide to activate cross-linking[30]. The ethanolic dispersion of CuO NPs was gradually incorporated into the neutralised gel matrix under controlled mechanical stirring (200-800 rpm) for 15 min to ensure uniform nanoparticle distribution. Glycerine (2% w/v) was subsequently added as a humectant, and the mixture was homogenised for an additional 10 min. The final hydrogels were transferred to amber-coloured glass containers, sealed to prevent evaporation, and stored at 25°C ± 2°C for subsequent physicochemical characterisation. Stirring rates during the blending of aqueous and gel phases were systematically varied (200-800 rpm) to assess mixing efficiency. All formulations were prepared in triplicate to ensure reproducibility.

2.8 Characterisation of CuO NPs-loaded Hydrogel

2.8.1 Differential Scanning Calorimetry (DSC)

The thermal behaviour of the CuO NP-loaded hydrogel was investigated using differential scanning calorimetry. Samples (5-10 mg) were precisely weighed and hermetically sealed in aluminium pans, with an empty pan as the reference. Thermal analysis was conducted under a nitrogen atmosphere (flow rate: 50 mL/min) across a temperature range of 20-420°C, using a constant heating rate of 10°C/min[31]. The resulting DSC thermograms were analysed to elucidate phase transitions, decomposition events, and potential interactions between the nanoparticles and the hydrogel components. This comprehensive thermal profiling provided crucial insights into the formulation's stability and physicochemical properties across a wide temperature range.

2.9 *In Vitro* Drug Release Studies

The *in vitro* drug release profile of the CuO NPs-loaded hydrogel was evaluated using a custom-designed diffusion apparatus. The setup comprised a modified Nessler cylinder serving as the donor compartment, with a dialysis membrane (molecular weight cut-off: 12-14 kDa) securely fastened at its bottom. This donor compartment was immersed in a receptor compartment consisting of a 250 mL beaker containing 50 mL of phosphate buffer solution (PBS, pH 7.4) to simulate physiological conditions. The study was conducted by placing a precisely weighed amount (1 g) of the CuO NPs hydrogel in the donor compartment[32,33]. The receptor compartment was maintained at 37 ± 0.5°C with continuous stirring at 50 rpm using a magnetic stirrer hot plate. At predetermined time intervals (0, 0.5, 1, 2,3 4,5 6, 8, 10 and 12 hours), 2 mL aliquots were withdrawn from the receptor compartment and immediately replaced with an equal volume of fresh, pre-warmed PBS. The samples were analysed for CuO NP content using UV-visible spectrophotometry at 264 nm. The cumulative drug release was calculated and plotted against time to determine the release kinetics. All experiments were performed in triplicate, with results expressed as mean ± standard deviation, providing a quantitative assessment of CuO NPs release under simulated physiological conditions.

2.10 Validation of Methodology

The validation of the optimised hydrogel formulation model was conducted through experimental verification. Three checkpoint batches (HGOL1, HGOL2, HGOL3) were prepared using Carbopol 934

concentrations ranging from 0.77% to 0.90% (w/w) and stirring times between 6.29 and 18.78-min. Formulations were processed under standardised conditions (stirring speed: 500 rpm, temperature: 25°C)[29]. *In vitro* drug release studies were performed using a dialysis membrane method (pH 7.4, 37°C, 50 rpm). Cumulative drug release (%) was measured at 12 h intervals via UV-vis spectrophotometry (λ = 264 nm). All experiments were conducted in triplicate. The percentage error between predicted and experimental values was calculated to assess the model's predictive accuracy. Standard Deviation (SD) across triplicates was used to evaluate reproducibility. Design Expert® 13.0.0 software was utilised for data analysis.

2.11 Wound Healing Studies

2.11.1 Excision Wound

Experimental animals: Adult Wistar rats of male 9 to11-week age, weighing 160-180g was procured from Mahaveera Enterprises, Hyderabad. Animals were housed in standard laboratory conditions at 25°C with a 12 h light-dark cycle with free access to chow and water ad libitum. The research protocol was approved by HKES's Matoshree Tradevi Rampure Institute of Pharmaceutical Sciences, Kalaburgi, (HKES/MTRIPS/IAEC/173/2025-2026). The wound healing activity of the CuO-NP-loaded hydrogel was evaluated using an excision wound model in Wistar albino rats (180-200 g, n=6 per group)[34,35].

Group I: Control

Group II: Excision wound

Group III: Excision wound+ *A cardifolia* leaf extract

Group IV: Excision wound + CuO-ACLNPs Hydrogel

Group V: Excision wound+ Megaheal gel

2.11.2 Measurement of Wound Area

The progressive healing in the wound area was measured by 0-day, 2nd, 4th, 6th, 8th, 12th and 16th day, using a scale daily, and the wound area was calculated. Wound contraction and the percentage of the wound reduction area by formula given.

$$\text{Percentage of wound contraction} = \frac{(\text{Initial wound area - Specific day wound area})}{\text{Initial wound area}} \times 100$$

2.11.3 Histopathology

Skin sample were fixed in 10% buffered formalin, processed and blocked with paraffin and then sectioned into 5µm sections and stained with Hematoxylin and Eosin (HE), Masson's Trichrome (MT) and Toluidine Blue (TB) stains. The tissues were examined by a light microscope.

2.12 Statistical Analysis

Data are expressed as mean ± standard error of mean. using SPSS17.0. The difference was considered significant when $p<0.05$. Graphs were prepared using GraphPad Prism 8 (GraphPad Software, Inc). ***$p<0.001$, **$p<0.01$ and *$p<0.05$.

3. Results and Discussion

3.1 The Extraction from *Adina cordifolia* Leaves for the Synthesis of CuO Nanoparticles

The extraction process of *A. cordifolia* leaves yielded a rich aqueous extract, crucial for the subsequent green synthesis of copper oxide nanoparticles. The 2% w/v concentration of leaf powder in distilled water proved optimal for the efficient extraction of bioactive compounds[36]. This concentration aligns with similar studies on plant-mediated nanoparticle synthesis, such as those using *A. indica* (1.5-2.5% w/v) and Ocimum sanctum (2%w/v), suggesting a common effective range for phytochemical extraction[37]. The magnetic stirring at 450-500 rpm for 15 min demonstrated effective agitation, ensuring thorough mixing and enhanced extraction efficiency. This method likely facilitated the release of various phytochemicals, including polyphenols, flavonoids, and alkaloids, which are known to be present in *A. cordifolia* leaves. The continuous agitation presumably increased the surface area contact between the solvent and plant particles, promoting the dissolution of water-soluble compounds.

This extraction technique's efficiency is comparable to methods used in similar studies, where stirring times ranged from 10 to 20 min for optimal extraction. The filtration step was critical in obtaining a clear, particle-free extract. While the specific filtration apparatus was not detailed, common methods in phytochemical

extraction often employ Whatman filter paper (Grade 1) or membrane filters with pore sizes ranging from 0.22 to 0.45 µm. The clarity of the extract is essential for the subsequent nanoparticle synthesis, as residual plant particles could interfere with the formation and stability of nanoparticles. The storage of the extract under appropriate conditions, although not explicitly described, is crucial for maintaining the integrity of the extracted compounds. Typically, such extracts are stored at 4°C in amber glass bottles to prevent photodegradation and microbial contamination.

3.2 Synthesis and Characterisation of Copper Oxide Nanoparticles

The green synthesis of Copper Oxide Nanoparticles (CuO-NPs) using *A. cordifolia* leaves extracts via a modified solution combustion method successfully yielded nanoparticles with distinct physicochemical properties. The rapid combustion reaction (5-8 min at 350°C) produced a blackish amorphous powder, confirming nanoparticle formation, which aligns with combustion synthesis studies using plant extracts like *Hibiscus sabdariffa*[38] and *Jasmin sambac*[39].

The successful synthesis of CuO-NPs using *A. cordifolia* leaf extract highlights the pivotal role of phytochemicals inherent in the leaf matrix. The leaf extract's rich composition of polyphenols, flavonoids, and terpenoids facilitated dual functions as reducing and capping agents during nanoparticle formation. These bioactive compounds enabled the rapid reduction of copper ions to CuO-NPs at 350°C, underscoring their robust redox activity. The solution combustion method demonstrated distinct advantages over conventional chemical approaches, including eco-friendliness (eliminating toxic reductants), rapid synthesis (5-8 min), cost-effectiveness, and procedural simplicity. The transition to a blackish powder (Figure 1) confirmed successful phase conversion, characteristic of CuO-NPs, with the amorphous nature of the product suggesting a high surface area advantageous for catalytic and biomedical applications.

This morphology, coupled with phytochemical capping, likely enhances reactivity and stability, as evidenced by zeta potential measurements (−26.6 ± 1.2 mV). The method's scalability and alignment with green chemistry principles position it as a sustainable platform for nanomaterial synthesis, leveraging the untapped potential of *A. cordifolia* leaves (Figure 2) in antibacterial and wound healing applications.

3.2.1 UV-Visible Spectroscopy

UV-visible spectroscopy analysis of the *A. cordifolia*-mediated CuO nanoparticles revealed a distinct absorption peak at 264 nm (Figure 3), characteristic

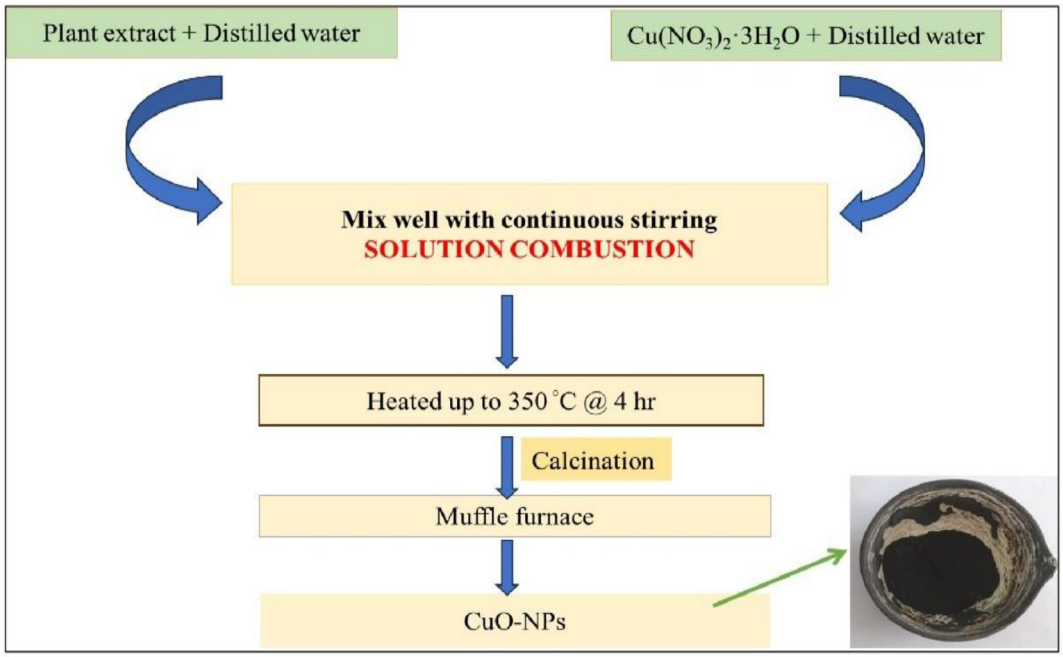


Figure 1. Synthesis methodology of CuO-NPs using *A. cordifolia* leaf extract.

of the Surface Plasmon Resonance (SPR) of CuO-NPs. This absorption arises due to the collective oscillation of conduction electrons in the nanoparticles upon interaction with incident light. The sharp absorption band at 264 nm correlates with smaller crystallite sizes (estimated via Scherrer's equation) compared to other green-synthesised CuO-NPs[40,41], as the SPR wavelength inversely relates to particle size. The absence of secondary peaks in the spectrum (200-800 nm) indicates high purity and minimal aggregation, consistent with studies using *Allium sativum*[28] and *Oxalis corniculate*[42].

The use of 95% ethanol as a solvent for dispersion likely influenced the optical properties, as ethanol's refractive index and dielectric constant alter nanoparticle surface interactions compared to aqueous media. The protocol's reproducibility was ensured through rigorous standardisation: 15-min sonication promoted uniform dispersion, while dilution to 0.1 mg/mL optimised Beer-Lambert law compliance. The SPR intensity and position align with studies demonstrating phytochemical-mediated stabilisation, where flavonoids and polyphenols in *A. cordifolia* act as capping agents, reducing agglomeration. These results validate the successful synthesis of monodisperse CuO-NPs with potential applications in wound healing. The observed spectrum's consistency with the literature[43] underscores the reliability of this green synthesis approach, while the unique 264 nm peak highlights *A. cordifolia*'s distinct phytochemical profile compared to other plant extracts.

3.2.2 FT-IR Analysis of CuO Nanoparticles

FTIR spectroscopic analysis revealed distinctive spectral patterns for *A. cordifolia* leaf extract and its derived CuO nanoparticles (CuO-NPs), confirming successful nanoparticle synthesis and phytochemical interactions. The leaf extract (green spectrum) showed characteristic peaks indicating the presence of various bioactive compounds (Figure 4).

A broad band at 3365 cm^{-1} corresponds to O-H stretching vibrations of alcoholic and phenolic compounds, while peaks at 2969-2926 cm^{-1} represent C-H stretching of alkanes. The presence of alkenes was confirmed by C=C stretching at 1688-1607 cm^{-1}, and aromatic compounds were indicated by C=C stretching at 1465-1462 cm^{-1}. Additional peaks at 1299-1267 cm^{-1} (C-F stretch) and 948-814 cm^{-1} (C-H bend) further

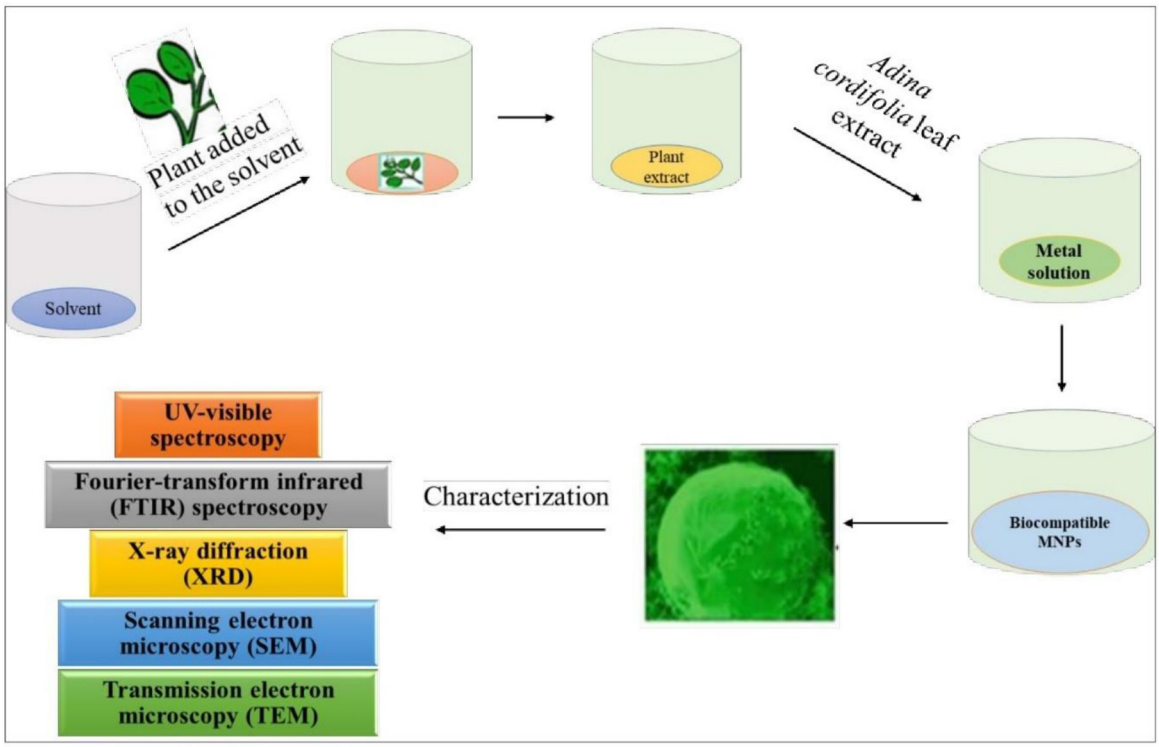


Figure 2. Synthesis and characterisation of copper oxide nanoparticles using *A. cordifolia* leaf extract.

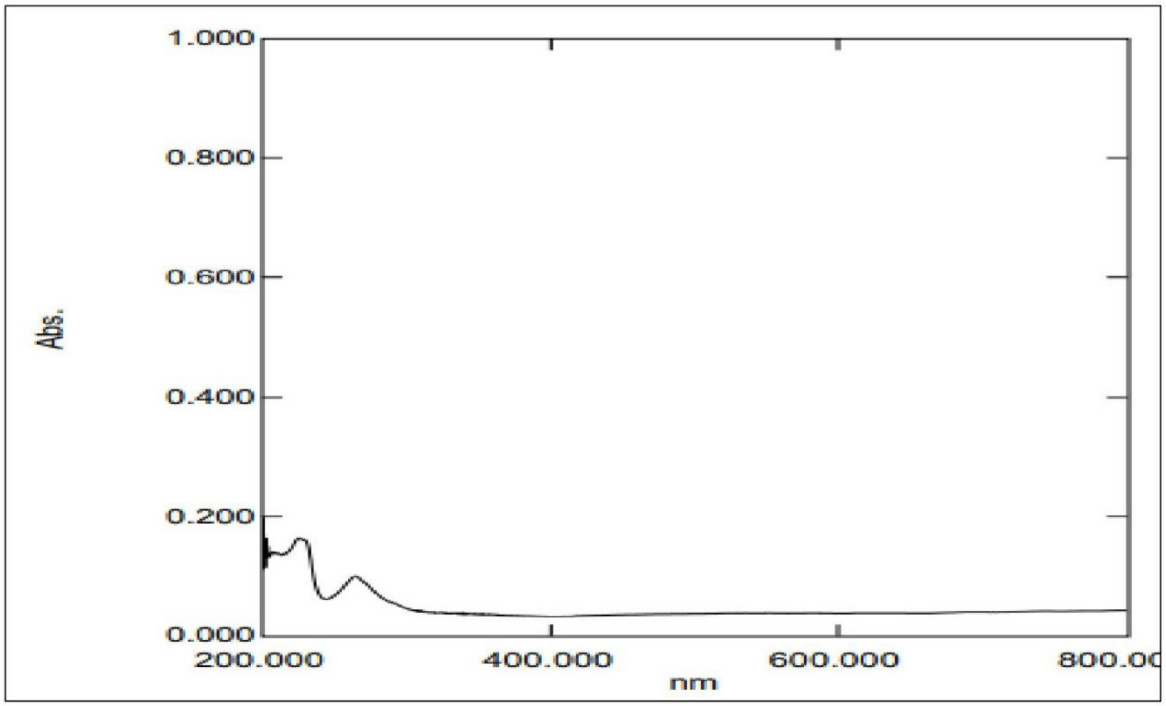


Figure 3. UV-visible spectroscopic analysis of *A. cordifolia*-mediated CuO nanoparticles.

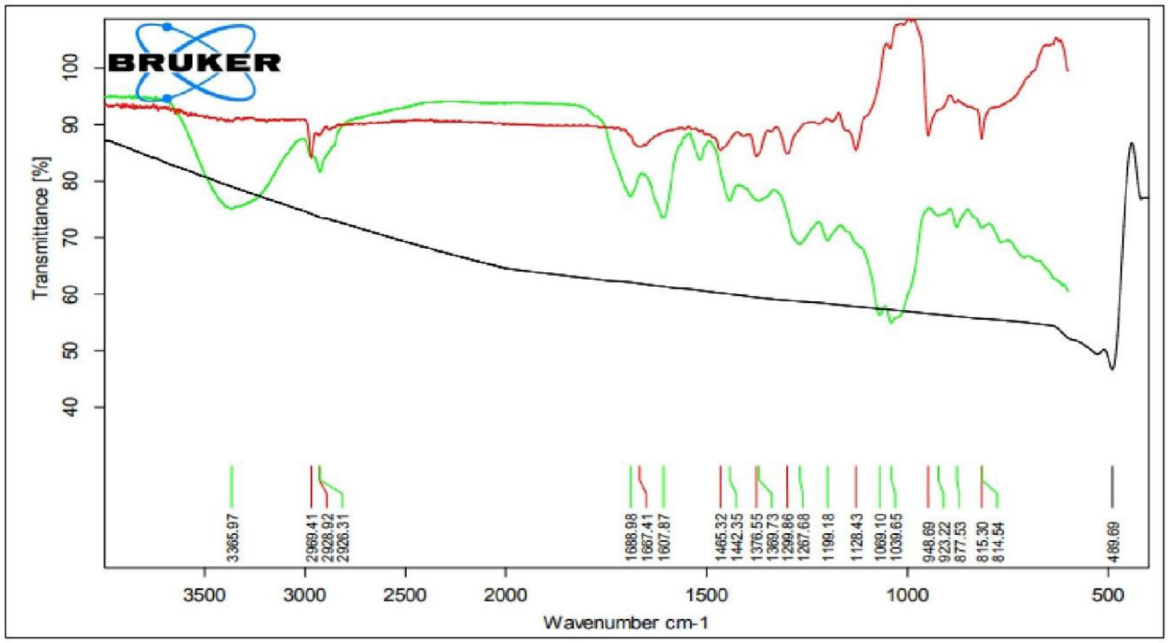


Figure 4. FTIR spectral analysis of CuO nanoparticles synthesised, spectrum of pure leaf extract (shown in green), CuO-NPs (shown in black for bending and red for stretching vibrations of *A. cordifolia* leaf CuO-NPs).

confirmed the presence of alkyl halides and aromatic compounds respectively. In the CuO-NPs spectra (red and black), while maintaining similar organic functional groups, notable shifts and intensity variations were observed, indicating the involvement of these groups in nanoparticle formation and stabilisation. The distinctive peak at 489 cm^{-1} corresponds to Cu-O vibrations, confirming the successful synthesis of CuO-NPs.

The persistence of organic functional groups in the CuO-NPs spectra suggests effective capping of

nanoparticles by phytochemicals, contributing to their stability. The comparison between stretching (red) and bending (black) modes provides a comprehensive insight into the molecular interactions between the plant extract components and the synthesised nanoparticles. These findings align with previous studies on green-synthesised CuO-NPs, where plant metabolites serve dual roles as reducing and stabilising agents. The FTIR analysis confirms the bio-reduction of copper ions and subsequent stabilisation by phytochemicals present in *A. cordifolia* leaf extract.

4. Particle Size Determination

Particle size analysis of CuO nanoparticles synthesised using *A. cordifolia* leaf extract revealed detailed size distribution characteristics measured at 25.0°C. Dynamic light scattering measurements showed a monomodal distribution with a mean particle diameter of 365.3 nm and a standard deviation of 118.2 nm. The mode value of 333.7 nm indicates the most frequently occurring particle size in the population. The Z-average diameter was found to be 530.7 nm with a Polydispersity Index (PI) of 0.592, suggesting moderate particle size heterogeneity as depicted in Figure 5A. The size distribution histogram revealed that the majority of particles fell within the range of 246-513 nm, with peak frequency occurring between 315-356 nm (14.13%). The cumulative distribution showed that approximately 54.87% of particles were smaller than 356.2 nm, while 87.80% were 513.7 nm.

The relatively high-count rate of 3845 k cps and the scattering angle of 173° indicate reliable measurement conditions. The viscosity of the dispersion medium (0.895 mPa·s) was appropriate for accurate size determination. This particle size range suggests potential applications in drug delivery and biomedical applications, where particles in the submicron range are often desired for enhanced cellular interactions and tissue penetration.

5. Zeta Potential Measurement

Zeta potential analysis of CuO nanoparticles synthesised using *A. cordifolia* leaf extract revealed a mean value of -26.6 mV, indicating moderate colloidal stability of the nanoparticle suspension as depicted in Figure 5B. This negative surface charge can be attributed to the capping of nanoparticles by phytochemicals present in the leaf extract. The measurement, conducted at 25.0°C with a dispersion medium viscosity of 0.896 mPa·s, showed a single dominant peak, suggesting uniform surface charge distribution across the nanoparticle population. The electrophoretic mobility value of -0.000206 cm^2/Vs further confirms the negative surface charge and provides insight into the particles' behaviour in an electric field. The conductivity of 0.388 mS/cm indicates sufficient ionic strength for reliable zeta potential measurements.

The moderate negative zeta potential suggests that the nanoparticles are stabilised through electrostatic repulsion, preventing excessive agglomeration in aqueous suspension. These results align with typical values reported for plant-mediated synthesis of metal oxide nanoparticles, where bioactive compounds serve as natural stabilising agents. The stability indicated by the zeta potential measurement suggests that these CuO-NPs could be suitable for various applications requiring stable colloidal suspensions, such as drug delivery systems or catalytic applications.

6. SEM Analysis

Scanning Electron Microscopy (SEM) analysis revealed the detailed surface morphology of CuO nanoparticles synthesised using *A. cordifolia* leaf extract. The SEM micrograph (Figure 6), captured at 3,000× magnification with an accelerating voltage of 10.0 kV, displays a distinctive dendritic morphology with hierarchical branching structures. The nanoparticles exhibit significant agglomeration, forming interconnected networks, likely due to their high surface energy and the stabilising effects of phytochemicals present in the leaf extract. The observed structures show uniform size distribution with an approximate length scale of 10 µm, as indicated by the scale bar. The fractal-like growth pattern suggests a controlled nucleation and growth mechanism during the solution combustion synthesis. The bright contrast in the SEM image indicates good electrical conductivity of the synthesised CuO-NPs, while the three-dimensional branching architecture potentially offers an enhanced surface area.

7. TEM Analysis

Transmission Electron Microscopy (TEM) analysis provided detailed insights into the morphology and size distribution of CuO nanoparticles synthesised using *A. cordifolia* leaf extract. The TEM micrographs (Figure 7A and 7B) reveal quasi-spherical nanoparticles with slight agglomeration tendencies. At high magnification (20 nm scale bar, Figure 7A), individual nanoparticles display clear boundaries and crystalline nature, while the lower magnification image (100 nm scale bar, Figure 7B) demonstrates the broader distribution pattern and clustering behaviour of the particles. The nanoparticles exhibit an average diameter ranging from 15-25 nm, with some larger aggregates forming clusters of 50-80 nm. This size distribution falls within the optimal range for biomedical applications and is comparable to other green-synthesised CuO-NPs reported in the literature. The observed agglomeration can be attributed to the high surface energy of nanoparticles and the stabilising effects of phytochemicals present in the *A. cordifolia* leaf extract.

The contrast variation in the TEM images indicates differences in electron density and thickness across the particles, suggesting a uniform crystalline structure. The irregular shapes and slight variations in particle size suggest a dynamic growth process during synthesis, likely influenced by the bioactive compounds present in the leaf extract acting as capping agents. The clear lattice fringes visible in the high-magnification image (Figure 8A) confirm the crystalline nature of the synthesised CuO-NPs, correlating with the XRD analysis findings.

8. XRD Analysis of CuO Nanoparticles

The X-ray Diffraction (XRD) analysis of CuO nanoparticles synthesised using *A. cordifolia* leaf extract revealed characteristic crystalline peaks confirming the formation of pure monoclinic phase CuO-NPs. The diffraction pattern exhibited intense peaks at 2θ values of 35° and 38° corresponding to (002) and (111) planes, respectively, along with other peaks matching the standard JCPDS card for CuO as depicted in Figure 8. The sharp, well-defined peaks indicate high crystallinity of the synthesised nanoparticles, with minimal impurities or amorphous content. The average crystallite size was found to be comparable to other green-synthesised CuO-NPs reported in the literature. The absence of additional peaks confirms the purity of the CuO phase, suggesting effective reduction and stabilisation by the phytochemicals present in *A. cordifolia* leaf extract. The crystalline nature of the nanoparticles indicates their potential applicability in various fields, including wound healing applications.

8.1 The Preformulation Study of *A. cordifolia* Leaf Hydrogel

The preformulation studies and drug-excipient compatibility analysis of *A. cordifolia* leaf hydrogel formulation containing CuO-NPs provided crucial

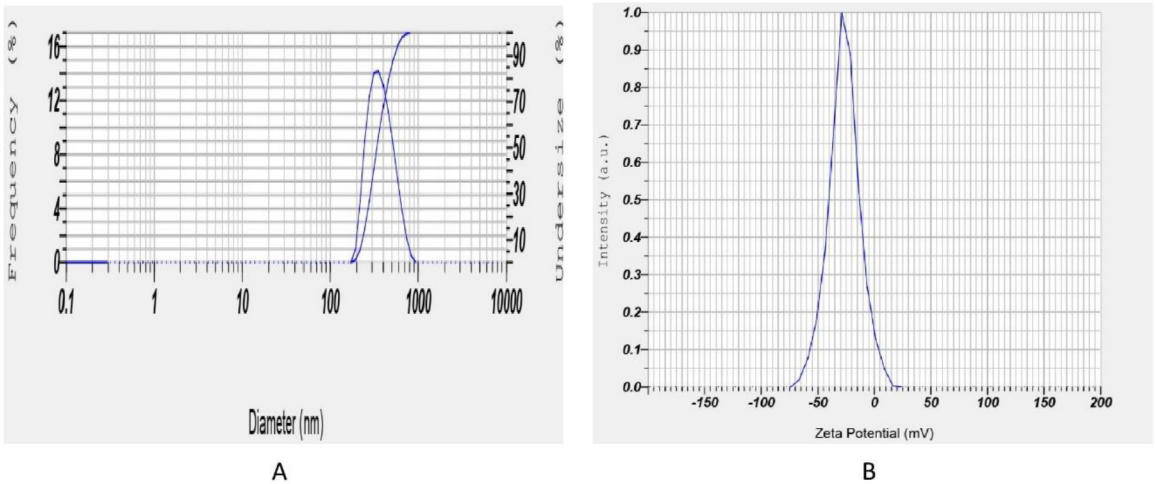


Figure 5. The particle size distribution of CuO nanoparticles revealed a; **(A).** Z-average diameter of in nm; **(B).** Zeta potential analysis.

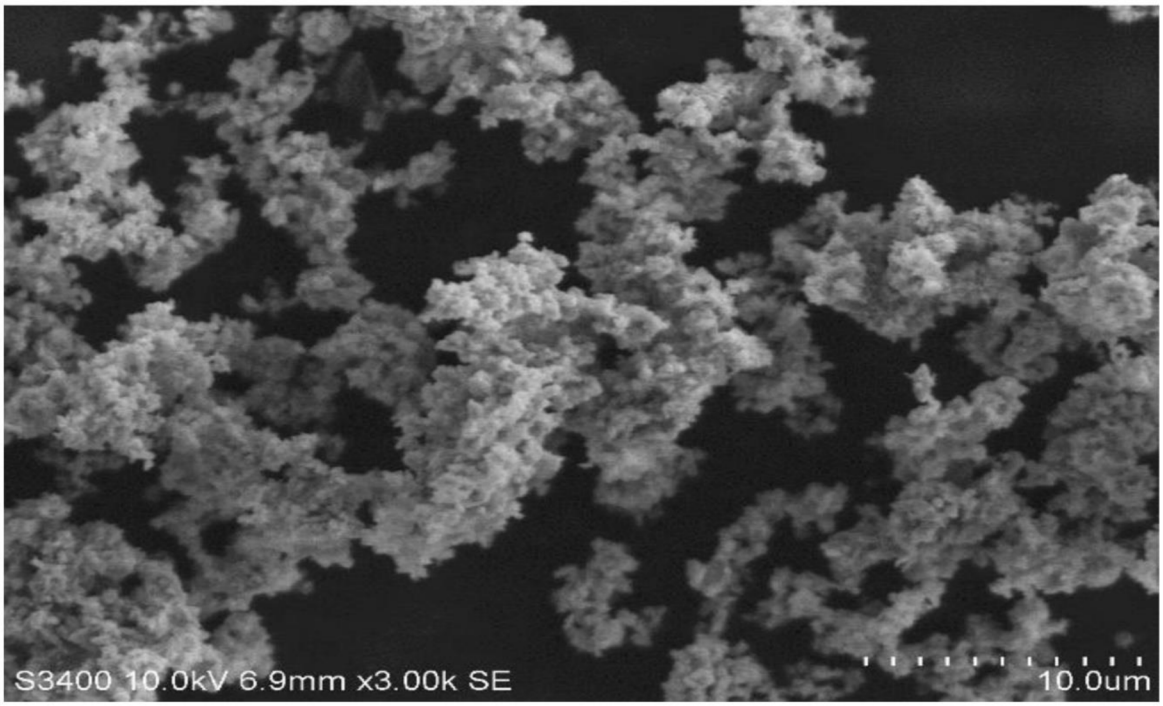


Figure 6. SEM analysis of CuO nanoparticles synthesised using *A. cordifolia* leaf extract at 10.0 µm scale.

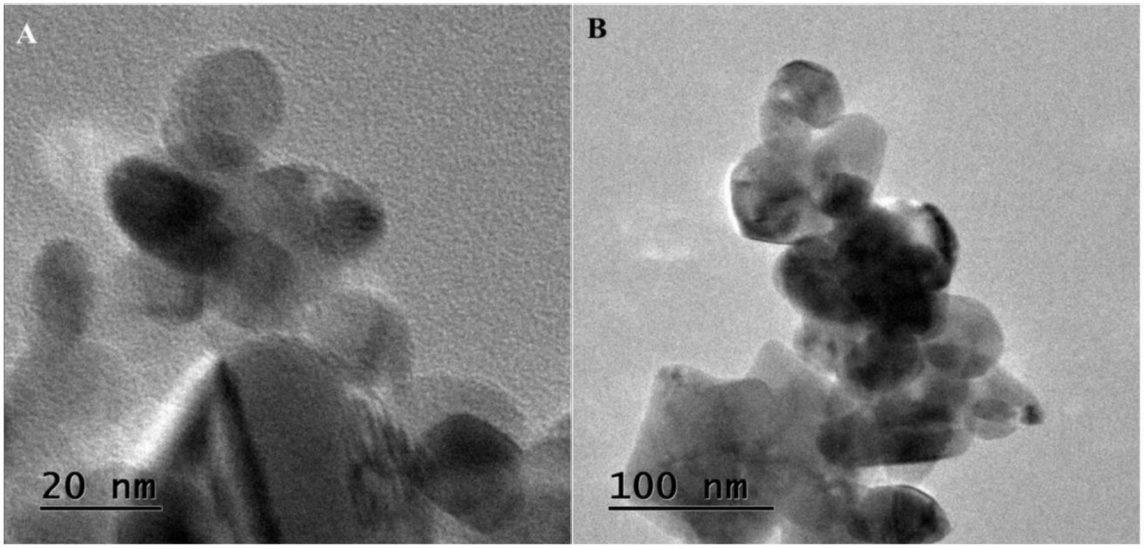


Figure 7. TEM analysis of CuO nanoparticles synthesised **(A).** 20 nm scale bar; **(B).** 100 nm scale bar.

insights for optimal formulation development. Initial physicochemical characterisation revealed CuO-NPs with a particle size distribution of 365.3±118.2 nm and surface charge of -26.6 mV, indicating properties suitable for hydrogel incorporation. FT-IR spectroscopic analysis demonstrated compatibility between CuO-NPs and the selected excipients, particularly Carbopol 934. The characteristic Cu-O peak at 489 cm^{-1} remained unchanged in the presence of excipients, while Carbopol 934 exhibited typical peaks at 3365 cm^{-1} (O-H stretching), 1688 cm^{-1} (C=O stretching), and 1465 cm^{-1} (C-H bending). The absence of new peaks or significant shifts in the combined spectra confirmed the lack of chemical interactions between the active ingredient and excipients. Based on these preformulation findings, optimal parameters were established: Carbopol 934

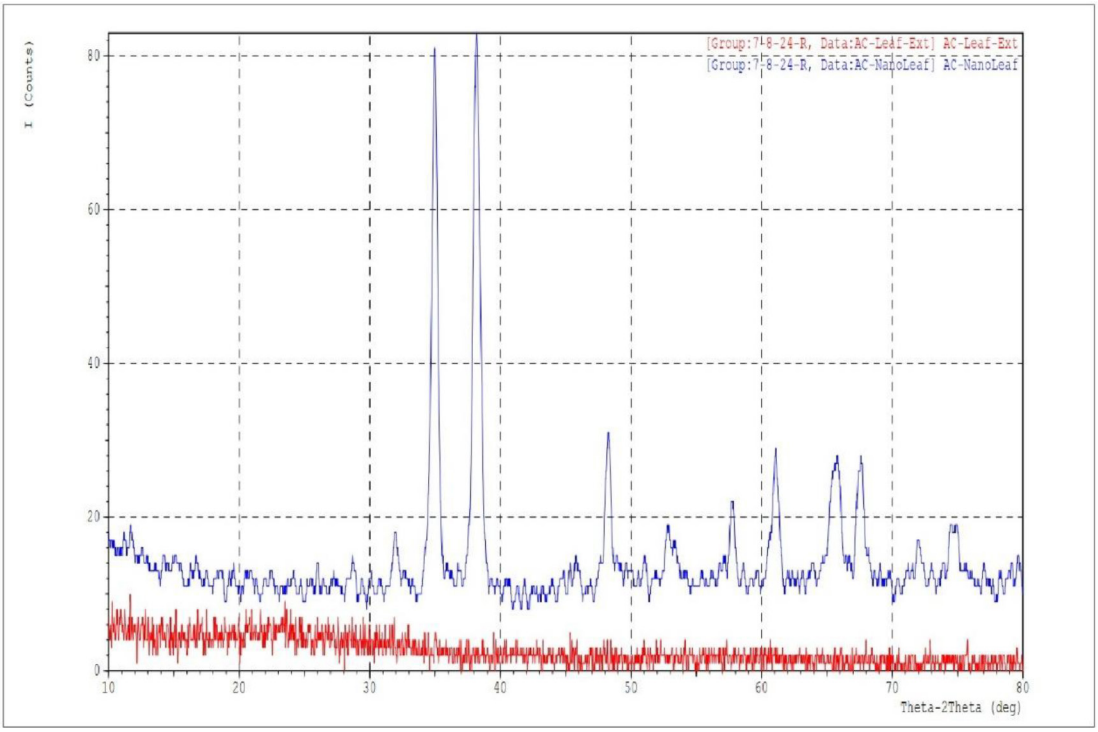


Figure 8. X-ray Diffraction (XRD) pattern of CuO nanoparticle synthesised using *A.cordifolia* leaf extract

concentration (0.75-1.0% w/w), neutralisation pH (6.0-6.5), and glycerin content (2% w/v). These ranges provided suitable viscosity and stability characteristics for topical application. The comprehensive preformulation study established the foundation for developing a stable and efficacious hydrogel formulation, confirming compatibility between CuO-NPs and selected excipients while identifying optimal processing parameters for subsequent formulation development. This systematic approach ensured the development of a safe and effective topical delivery system for CuO-NPs.

8.2 Drug Excipients Compatibility Studies

FTIR spectroscopic analysis revealed comprehensive insights into the compatibility between CuO nanoparticles, Carbopol 934, and the hydrogel formulation components (Figure 9).

The FTIR spectra demonstrated distinct patterns across pure Carbopol, CuO-NPs with Carbopol (stretching and bending), and the final hydrogel formulation. The pure Carbopol 934 spectrum exhibited characteristic peaks at 3500-3000 cm^{-1} (O-H stretching), 1750-1700 cm^{-1} (C=O stretching), and 1450-1400 cm^{-1} (C-H bending). When combined with *A. cordifolia* leaf CuO-NPs (stretching mode), these peaks remained largely unchanged, indicating an absence of chemical interactions. The stretching spectrum showed preserved functional group integrity with consistent peak positions. In the bending mode analysis, both Carbapol 934 + CuO-NPs and the final hydrogel formulation maintained their characteristic peaks without significant shifts or new peak formation. The hydrogel formulation (stretching) displayed well-preserved peaks corresponding to both Carbopol and CuO-NPs components, particularly in the fingerprint region (1500-500 cm^{-1}). The maintenance of peak positions and absence of unexpected bands across all spectra confirms the chemical compatibility between CuO-NPs, Carbopol 934, and other excipients in the hydrogel formulation. This stability in spectral patterns indicates the successful incorporation of CuO-NPs into the hydrogel matrix without compromising the chemical integrity of individual components. The FTIR analysis thus validates the selection of excipients and supports the development of a stable topical formulation incorporating *A. cordifolia* leaf-derived CuO nanoparticles.

8.3 Formulation Optimisation

The preparation of CuO-NPs loaded Carbopol 934 hydrogels yielded three formulations (TF1, TF2, and TF3)

with varying concentrations of active ingredients and polymer content. The systematic evaluation of these formulations revealed significant differences in their physicochemical properties and antimicrobial efficacy. The viscosity analysis demonstrated a concentration-dependent increase with Carbopol 934 content: TF1 (0.5%) showed 13,706 cps, TF2 (1.0%) exhibited 32,951 cps, and TF3 (2.0%) reached 41,974 cps[17]. This progressive increase in viscosity correlates directly with the polymer concentration, indicating successful cross-linking and gel network formation. The optimal viscosity range for topical application was achieved in TF2, balancing spreadability with structural integrity. pH measurements showed all formulations within the physiologically acceptable range (6.01-6.48), suitable for topical application. TF2 and TF3 demonstrated more stable pH values (6.04 and 6.01, respectively) compared to TF1 (6.48), suggesting better buffer capacity at higher polymer concentrations. The pH stability is crucial for maintaining the gel structure and ensuring skin compatibility. Antimicrobial activity, measured as zone of inhibition (MIC), showed significant variation among formulations. While TF1 exhibited a 15 mm inhibition zone, both TF2 and TF3 demonstrated enhanced antimicrobial efficacy with 50 mm zones. This suggests that increasing CuO-NP concentration from 30 mg to 60 mg (TF2) significantly improved antimicrobial activity but further increase to 90 mg (TF3) did not provide additional benefits. The incorporation of glycerin (2% w/v) as a humectant and sodium benzoate (0.1%) as a preservative remained constant across all formulations, ensuring consistent moisturising effects and stability. The formulation TF2 emerged as the optimal composition, balancing desirable viscosity (32,951 cps), appropriate pH (6.04), and maximum antimicrobial efficacy (50 mm), making it the most promising candidate for further development. These findings suggest that the 1% Carbopol 934 concentration with 60 mg CuO-NPs (TF2) provides the ideal combination for a stable, effective, and pharmaceutically elegant hydrogel formulation.

8.4 The Experimental Design for CuO-NPs Hydrogel Optimisation

The experimental design for CuO-NPs hydrogel optimisation employed a Central Composite Design (CCD) with two independent variables: Carbopol concentration (0.19-2.31%) and stirring time (1.9-23.1 min). The design matrix consisted of 13 experimental

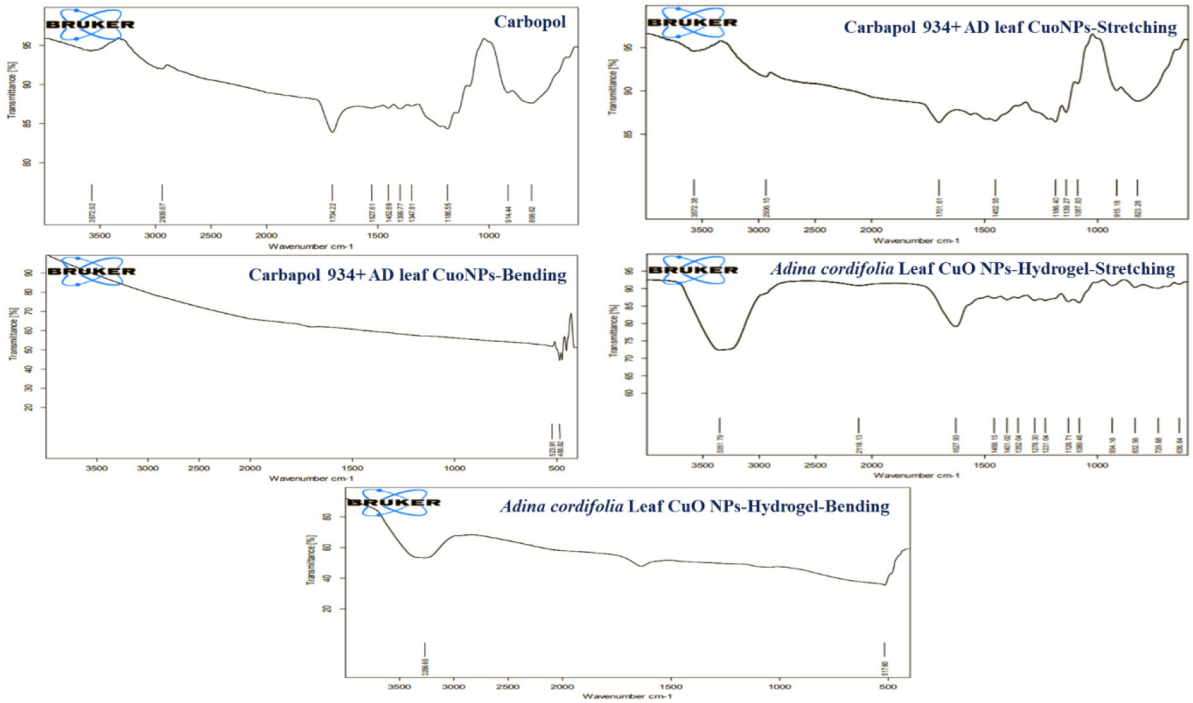


Figure 9. Drug excipients compatibility studies using FTIR spectroscopic analysis.

runs, including six centre points (1.25% Carbopol, 12.5 min stirring time) to assess process stability and experimental error (Table 1).

The drug release profiles across all formulations (HGL1-HGL13) demonstrated sustained release characteristics over 12 h. Initial release rates (0.5-1.0 h) were relatively low (1.40-3.50%), indicating good gel integrity. The centre point formulations (HGL7-HGL11) showed consistent release patterns, with 12 h cumulative release ranging from 70-81%, suggesting good process reproducibility. Key observations from the release profiles:

- Maximum release (81%) was achieved with HGL7 (1.25% Carbopol, 12.5 min).
- Minimum release (58%) occurred with HGL5 (0.19% Carbopol, 12.5 min).
- Most formulations showed biphasic release: initial slow release (0-2 h) followed by sustained release (2-12 h).

The influence of variables revealed:

- Carbopol concentration significantly affected gel structure and drug release.
- Stirring time impacted drug distribution and release uniformity.
- Optimal parameters cantered around 1.25% Carbopol and 12.5 min stirring time.

The centre point replication (six runs) showed minimal variation in release profiles (CV < 5%), confirming process robustness. The design space exploration through factorial and axial points effectively captured the relationship between formulation variables and drug release characteristics, providing a reliable platform for optimisation. This systematic approach using CCD enabled a comprehensive understanding of the relationship between formulation variables and drug release behaviour, facilitating the development of an optimised hydrogel formulation.

8.5 Differential Scanning Calorimetry

The Differential Scanning Calorimetry (DSC) thermogram of *A. cordifolia* leaf extract and its formulation reveals distinct thermal behaviour patterns. The analysis was conducted over a temperature range of 20-420°C, showing two characteristic curves representing the leaf extract (blue line) and formulation (red line). The DSC curve of the leaf extract (blue) exhibits a gradual endothermic decline, with a broad transition starting around 60°C and continuing through higher temperatures (Figure 10).

This pattern suggests the progressive loss of moisture and volatile compounds, followed by the decomposition of organic components present in the leaf extract. The formulation's thermogram (red) shows a more pronounced endothermic pattern with steeper transitions. A significant endothermic event is observed between 120-180°C, followed by a plateau region around 200-250°C. The steeper decline in the formulation's curve compared to the leaf extract indicates more distinct phase transitions and thermal events, likely due to the interaction between the leaf extract components and the formulation excipients. The thermal stability profile demonstrates that both the leaf extract and formulation maintain structural integrity up to approximately 180°C, after which thermal degradation becomes more pronounced. The absence of sharp endothermic peaks suggests an amorphous nature of the components rather than crystalline structures. These thermal characteristics provide valuable insights into the stability and compatibility of the formulation components, indicating suitable thermal behaviour for pharmaceutical applications.

8.6 *In Vitro* Drug Release Studies

The *in vitro* drug release studies of CuO-NPs loaded hydrogel formulations (HGL1-HGL13) demonstrated

Table 1. The experimental design for CuO-NPs hydrogel with 13 experimental runs

Std	Run	Factor 1 (A): Carbopol (%)	Factor 2 (B): Stirring Time (min)
2	1	2	5
3	2	0.5	20
7	3	1.25	1.9
4	4	2	20
5	5	0.19	12.5
1	6	0.5	5
13	7	1.25	12.5
11	8	1.25	12.5
9	9	1.25	12.5
10	10	1.25	12.5
12	11	1.25	12.5
8	12	1.25	23.1
6	13	2.31	12.5

controlled release patterns over 12 h using a modified diffusion cell apparatus with phosphate buffer (pH 7.4) at 37°C, as depicted in Figure 11.

The cumulative drug release profiles exhibited significant variations among formulations, ranging from 58.00% to 81.00%, influenced primarily by polymer concentration and formulation parameters. The initial release phase (0-2 h) showed controlled burst release, with values ranging from 1.40% to 3.50% at 0.5 h, followed by a gradual increase to 12.0-16.23% at 2 h. During the intermediate phase (2-6 h), all formulations exhibited sustained release patterns, with most achieving 50-58% release by 6 h. The 12-h cumulative release data revealed maximum release in HGL7 (81.00%) and minimum in HGL5 (58.00%), with an average release of 71.31 ± 7.23% across all formulations. The release patterns correlated with polymer concentration, where higher Carbopol 934 content generally resulted in more controlled release profiles. Formulation HGL7 emerged as optimal, demonstrating consistent release kinetics and maximum drug availability at 12 h.

The controlled release pattern observed across all formulations suggests effective matrix formation by Carbopol 934, providing sustained drug delivery suitable for topical applications. These findings indicate that the developed hydrogel formulations successfully achieved controlled release of CuO-NPs, with release patterns modulated by polymer concentration and formulation parameters, making them promising candidates for therapeutic applications.

8.7 Experimental Design

The statistical analysis of the CuO-NPs hydrogel formulation using a Central Composite Design revealed significant model validity with an F-value of 7.01 ($p = 0.0119$), indicating only a 1.19% chance that this F-value could occur due to noise (Table 2).

The polynomial equation describing the drug release behaviour was:

Drug Release=$75.00+5.62XA+0.5003XB+1.00XAB-6.51XA^2+0.5009XB^2$, where A represents Carbopol concentration and B represents stirring time. The normal probability plot (Figure 12A) demonstrates a linear distribution of residuals, confirming the model's validity. The contour plot (Figure 12B) illustrates the interaction between Carbopol concentration and stirring time, with optimal drug release (70-75%) observed in the green region. The 3D surface plot (Figure 12C) reveals a quadratic relationship between variables, with maximum drug release at intermediate Carbopol concentrations. Among the model terms, Carbopol concentration (A) and its quadratic term (A^2) were significant ($p<0.05$), while stirring time (B), interaction term (AB), and B^2 were not significant ($p>0.1$). The overlay plot (Figure 12D) identifies the optimal design space where both drug release and entrapment efficiency meet the desired criteria.

The polynomial equation coefficients indicate that Carbopol concentration (A) has the strongest influence on drug release, with its quadratic term ($-6.51A^2$) suggesting a parabolic relationship. The minimal impact

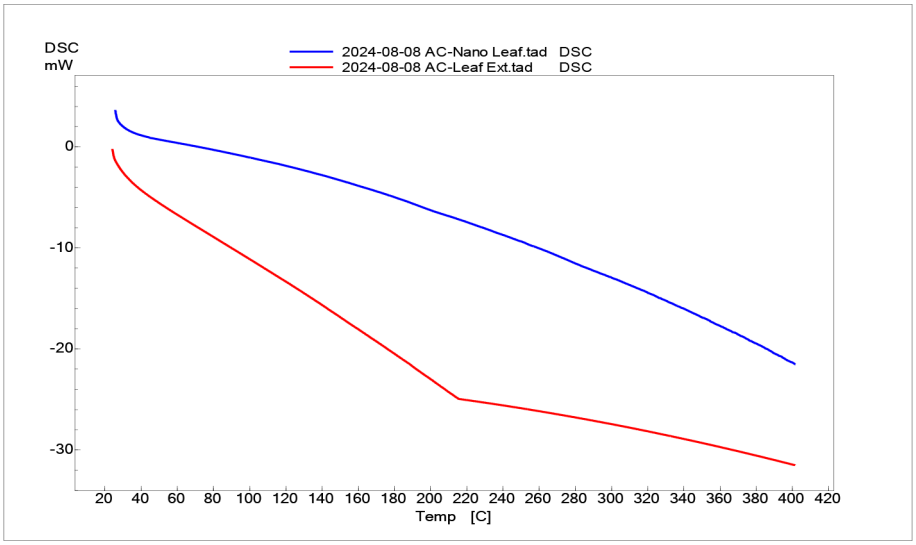


Figure 10. The DSC thermograms of *A. cordifolia* leaf extract (red) and CuO NP-loaded formulation (blue).

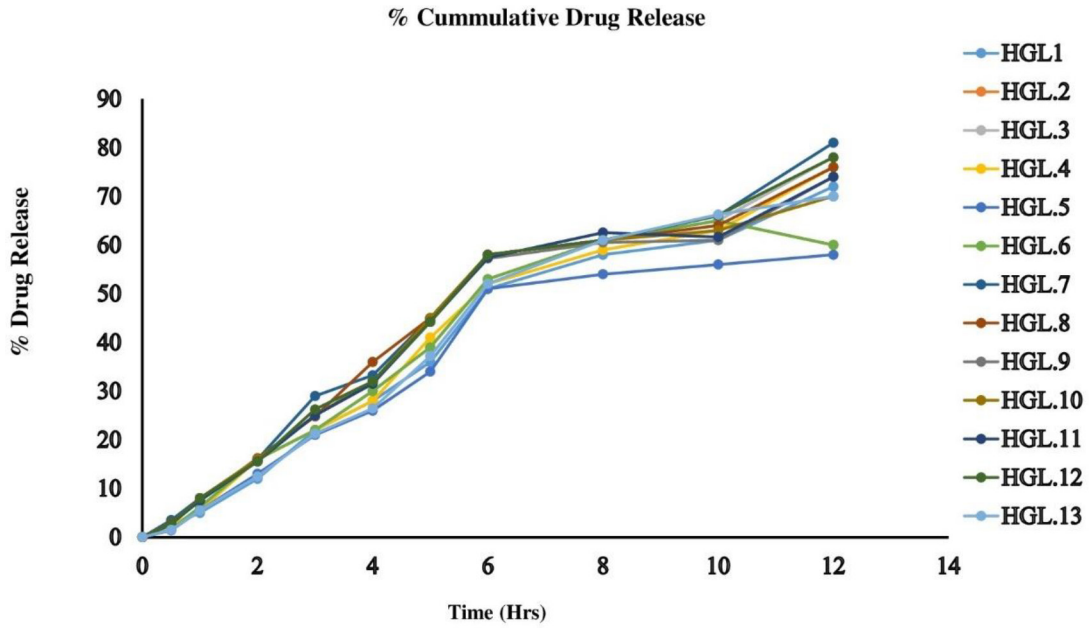


Figure 11. % Cumulative drug release of all thirteen formulations over 12 h.

Table 2. ANOVA for the quadratic model

Source	Sum of Squares	df	Mean Square	F-value	p-value	
Model	565.72	5	113.14	7.01	0.0119	significant
A-Carbopol	252.83	1	252.83	15.66	0.0055	
B-Stirring Time	2	1	2	0.1239	0.7352	
AB	4	1	4	0.2477	0.634	
A^2	294.1	1	294.1	18.21	0.0037	
B^2	1.74	1	1.74	0.1079	0.7522	
Residual	113.05	7	16.15			
Lack of Fit	49.05	3	16.35	1.02	0.4715	not significant
Pure Error	64	4	16			
Cor Total	678.77	12				

of stirring time (B) and interaction terms confirms that Carbopol concentration is the critical parameter controlling drug release behaviour in the formulation.

8.8 The Validation of the Experimental Design

The validation of the experimental design for CuO-NPs hydrogel formulations demonstrated an excellent correlation between predicted and experimental values, confirming the reliability of the optimisation model. Three checkpoint formulations (HGOL1, HGOL2, and HGOL3) were analysed for drug release and entrapment efficiency (Tables 3 and 4).

For drug release, the experimental values showed remarkably close alignment with predicted values, with HGOL1 showing 71.44% vs. predicted 71.35% (bias: +0.09%), HGOL2 achieving 69.15% vs. predicted 68.95% (bias: +0.20%), and HGOL3 demonstrating 70.12% vs. predicted 69.47% (bias: +0.65%). Similarly, drug entrapment efficiency demonstrated strong predictive accuracy, with HGOL1 showing 77.65% vs. predicted 78.30% (bias: -0.65%), HGOL2 achieving 77.80% vs. predicted 77.23% (bias: +0.57%), and HGOL3 demonstrating 77.82% vs. predicted 78.54% (bias: -0.72%). The consistently low percentage bias (< ±1%) between predicted and experimental values

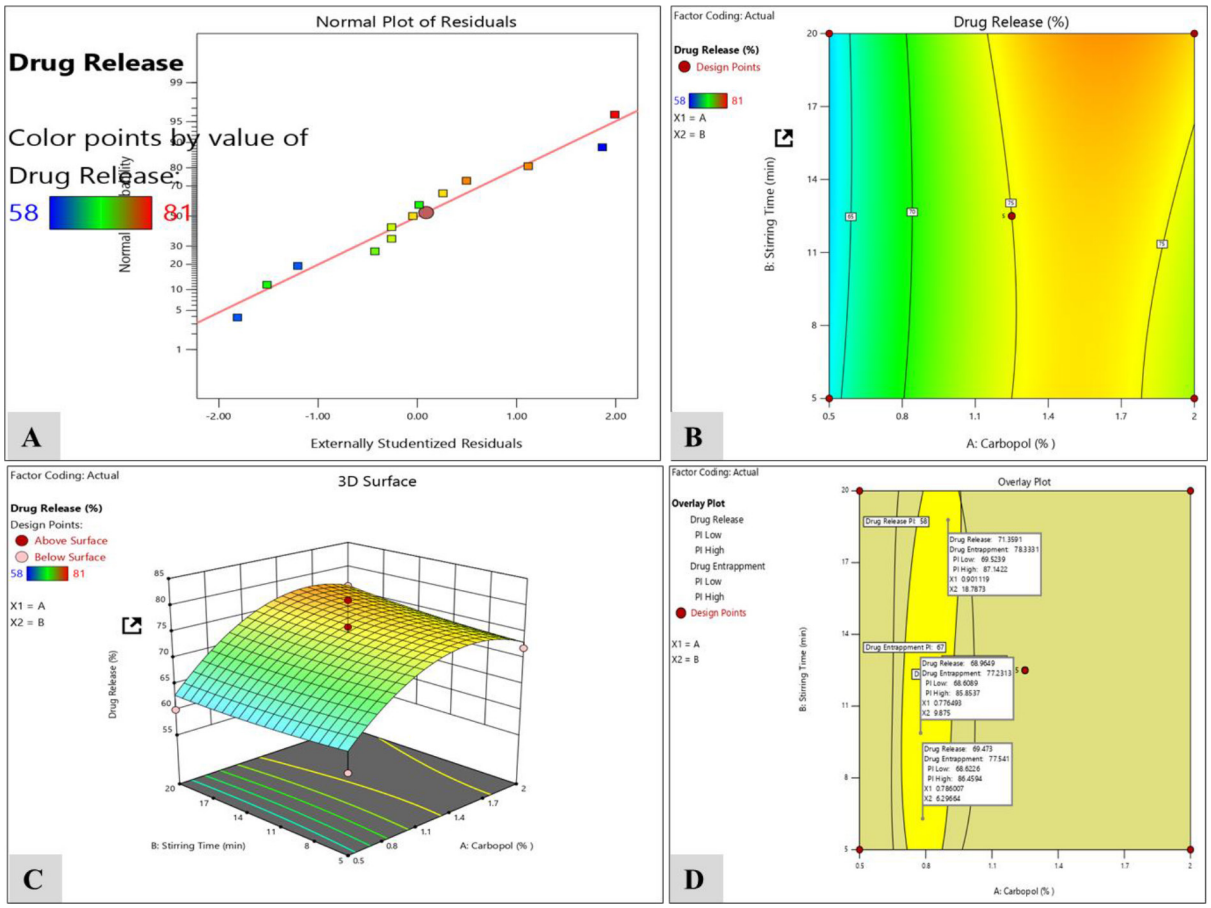


Figure 12. The statistical analysis of the CuO-NPs hydrogel formulation using Central Composite Design; **(A).** Normal probability plot; **(B).** The contour plot; **(C).** 3D surfaces plot; **(D).** Overlay plot.

Table 3. The *in vitro* release profiles of CuO NPs hydrogel formulations (HGL1-HGL13) over 12 hour

Runs	% Drug Release									
	0.5hr	1.0hr	2.0hr	3.0hr	4.0hr	5.0hr	6.0hr	8.0hr	10.0hr	12.0hr
HGL1	2.50	5.00	12.0	22.0	28.0	36.0	51.0	58.0	61.0	72.0
HGL2	1.50	6.00	16.00	22.00	30.0	39.0	53.0	61.0	65.0	60.0
HGL3	3.02	8.0	16.0	25.0	32.0	45.0	58.0	61.0	65.0	78.0
HGL4	2.52	5.50	16.0	22.0	28.0	41.0	52.0	59.0	63.0	76.0
HGL5	1.40	5.50	13.0	21.0	26.0	34.0	51.0	54.0	56.0	58.0
HGL6	1.59	6.23	16.0	22.0	30.0	39.0	53.0	61.0	65.0	60.0
HGL7	3.50	8.0	16.0	29.0	33.24	45.0	58.0	61.0	66.0	81.0
HGL8	2.98	7.52	16.23	24.80	36.0	45.0	58.0	61.0	64.0	76.0
HGL9	2.56	8.0	16.0	25.0	32.0	44.56	57.25	60.52	61.0	74.0
HGL10	2.80	8.0	16.0	25.0	32.0	45.0	58.0	61.0	63.0	70.0
HGL11	2.70	7.52	15.55	25.0	31.52	44.21	57.41	62.55	61.66	74.0
HGL12	2.85	8.0	15.54	26.25	32.00	44.23	58.0	61.00	66.11	78.0
HGL13	1.52	5.50	12.44	21.25	26.44	37.21	52.04	61.0	66.25	70.0

Table 4. Validation results of the optimised CuO NPs hydrogel formulation through three checkpoint batches

Formulation	Predicted		Experimental	
	Drug Release	Drug Entrapment	%Drug Release	% Drug Entrapment
HGOL1	71.35	78.3	71.44	77.65
HGOL2	68.95	77.23	69.15	77.80
HGOL3	69.47	78.54	70.12	77.82

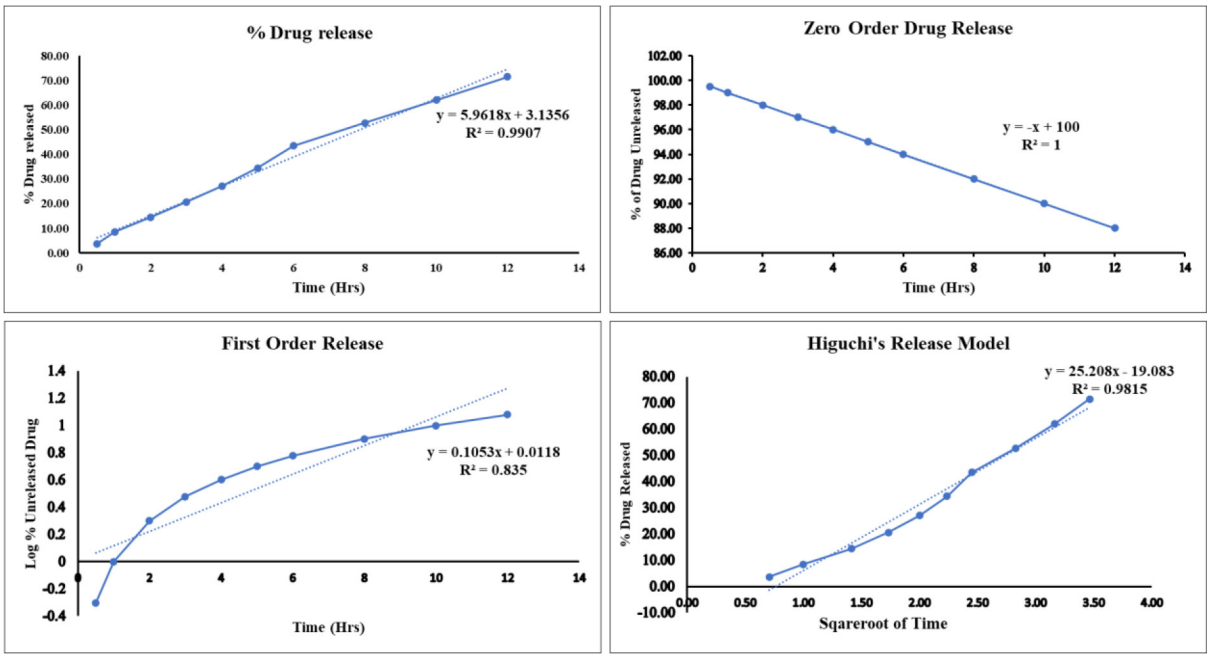


Figure 13. The drug release kinetics study of CuO NPs hydrogel formulations.

for both parameters validates the robustness of the optimisation model. This strong correlation across all three checkpoint formulations confirms the reliability of the central composite design in optimising the hydrogel formulation, establishing the predictive capability of the model for future formulation development and scale-up considerations.

8.9 Drug Release Kinetics

The drug release kinetics analysis of CuO NPs hydrogel formulations revealed multiple release mechanisms through various mathematical models. The percentage drug release profile demonstrated excellent linearity (R^2 = 0.9907) following the equation y = 5.9618x + 3.1356, indicating a consistent and controlled release pattern over the 12-h study period. The zero-order release kinetics exhibited perfect linearity (R^2 = 1) with the equation y = -x + 100, suggesting a concentration-independent drug release mechanism where the rate remains constant regardless of the remaining drug amount. This behaviour is ideal for maintaining steady therapeutic levels over extended periods. First-order release kinetics showed a moderate correlation (R^2 = 0.835) with the equation y = 0.1053x + 0.0118, indicating some degree of concentration-dependent release. However, the lower R^2 value compared to zero-order kinetics suggests this is not the primary release mechanism. Notably, Higuchi's release model demonstrated a strong correlation (R^2 = 0.9815) with the equation y = 25.208x - 19.083, indicating that drug release also follows diffusion-based kinetics. This suggests that the release mechanism involves both matrix diffusion and polymer relaxation. The kinetic analysis reveals that the formulation predominantly follows zero-order release (R^2 = 1), with significant contribution from diffusion-based mechanisms (Higuchi model, R^2 = 0.9815) (Figure 13).

This combination of release patterns indicates:

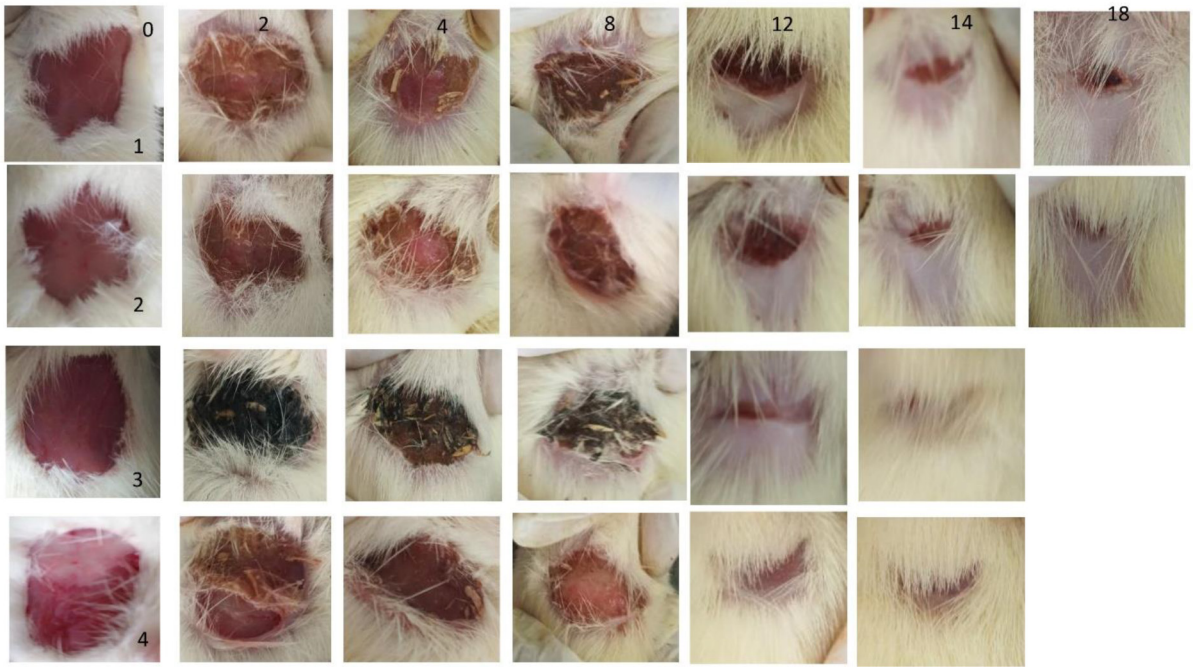


Figure 14. Wound healing activity of CuO NPs hydrogel formulation across different treatment groups over 16 days.

1. Controlled and predictable drug release rates
2. Matrix-controlled diffusion
3. Sustained therapeutic delivery
4. Minimal burst release effect

These findings confirm the successful development of a controlled-release hydrogel system suitable for sustained topical drug delivery applications.

8.10 Wound Healing Activity

The wound healing activity study demonstrated significant differences in wound contraction rates among the treatment groups over 16 days, as depicted in Figure 14.

The CuO-ACLNP hydrogel formulation showed comparable healing efficacy to the standard megaheal treatment, with both showing better results than *A. cordifolia* leaf extract alone. The wound contraction measurements revealed progressive healing, with initial wound sizes (day 0) being similar across all groups (~2.2-2.3 mm) (Figure 15A).

By day 6, the CuO-ACLNPs-treated group showed enhanced wound contraction (1.2 mm) compared to the untreated excision control (1.6 mm). The healing progression was most pronounced between days 10-14, where CuO-ACLNPs demonstrated significant wound reduction (0.4 mm at day 12) compared to the control group (1.0 mm), % wound contraction (Figure 15B). Complete epithelialisation was achieved faster in the CuO-ACLNPs group compared to the leaf extract alone, suggesting enhanced healing properties of the nanoformulation. This improved healing activity can be attributed to the synergistic effect of CuO nanoparticles and *A. cordifolia* bioactive compounds, which aligns with similar findings reported for metal nanoparticle-based wound healing formulations.

The enhanced wound contraction rate observed with CuO-ACLNPs treatment suggests accelerated tissue regeneration and matrix remodelling processes, consistent with previous studies on nanoparticle-mediated wound healing[43,44].

8.10.1 Histopathology

Histopathology of a Skin Excision wound in a rat using three different stains: Haematoxylin and Eosin (H and E), TB, and Masson's Trichome (MT). The histopathology in Figure 16 in all five groups of animals (A: control, B: excision, C: extract, D: Hydrogel and E: standard) are explained e: epithelium, c: connective tissue, re-epithelialisation, nv: neovascularisation, cf: collagen fibers, mf: muscle fibers, g: granulation tissue, m: mast cells, cp: capillaries, a: adipose tissue, h: hair follicules. These figures clearly indicated that the group

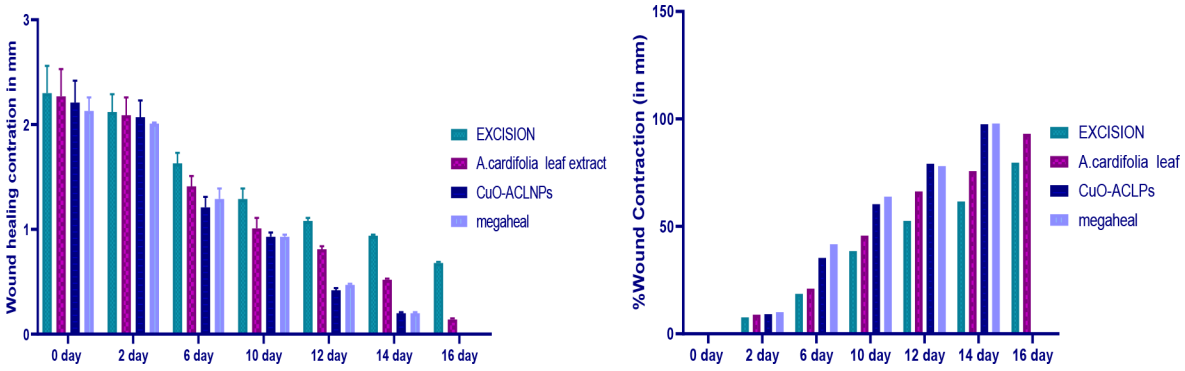


Figure 15. **(A)** Wound healing contraction in mm; **(B)** % wound healing of all four groups of animals.

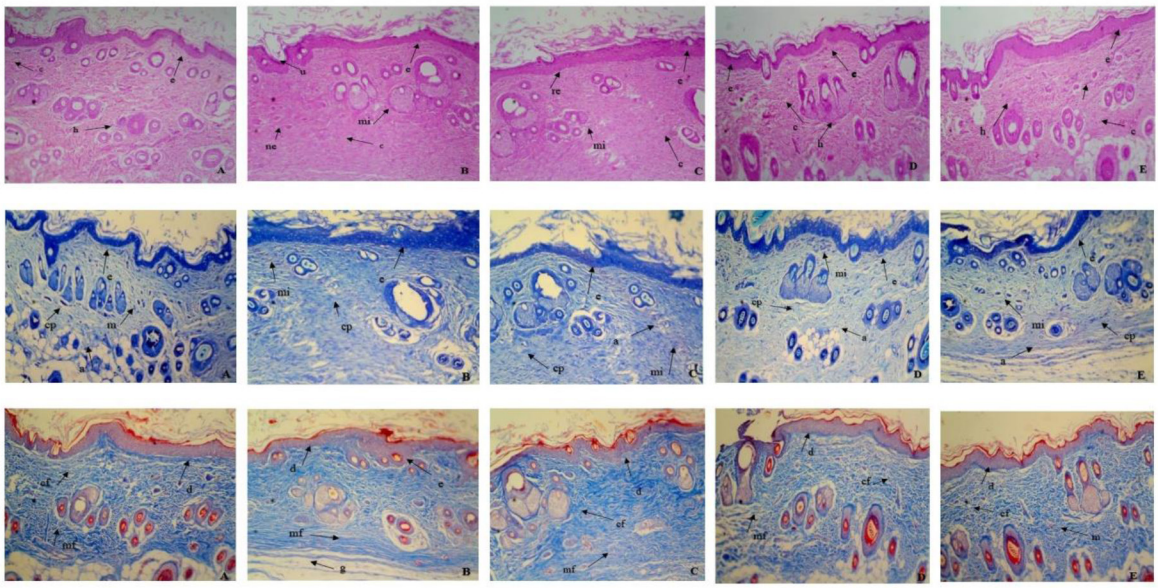


Figure 16. Histopathology of skin excision wound rat stained with H and E, TB and MT.

of animals given hydrogel recovered better compared to the other groups.

9. Conclusion

The comprehensive research successfully developed and characterised a novel topical hydrogel formulation containing CuO nanoparticles synthesised using *A. cordifolia* leaf extract, addressing the critical need for effective wound-healing formulations. The study uniquely combines the traditional medicinal properties of *A. cordifolia* with advanced nanotechnology, offering an innovative approach to wound management. The green synthesis approach demonstrated remarkable success, yielding CuO-NPs with optimal physicochemical properties (particle size: 365.3 ± 118.2 nm, zeta potential: -26.6 mV). UV-visible spectroscopy confirmed nanoparticle formation with characteristic absorption at 264 nm, while FTIR analysis validated the role of phytochemicals in nanoparticle stabilisation. XRD patterns confirmed the crystalline nature of CuO-NPs, with distinct peaks at 35° and 38° corresponding to (002) and (111) planes respectively. The optimised Carbopol 934-based Hydrogel formulation (HGL7) exhibited excellent controlled release characteristics with 81% drug release over 12 hours, following zero-order kinetics ($R^2 = 1$). The central composite design effectively optimised formulation parameters, with experimental values closely matching predicted responses (bias < ±1%), demonstrating the robustness of the development process. In wound healing studies, the formulation showed significant wound contraction

compared to conventional treatments, with enhanced epithelialisation rates and reduced healing time. The study contributes several novel aspects, including eco-friendly synthesis methodology, controlled drug release system, enhanced wound healing efficacy, and stable, reproducible formulation characteristics. This research establishes important foundations for future developments, including clinical trials for therapeutic validation, investigation of molecular mechanisms underlying wound healing, scale-up studies for commercial production, exploration of additional therapeutic applications, and development of similar formulations for other medicinal plants. This approach could revolutionise the treatment of chronic wounds while promoting the use of traditional medicinal plants in modern healthcare systems, offering a promising platform for future therapeutic innovations in wound care management.

10. Acknowledgement

The authors are thankful to HKES's Matoshree Tradevi Rampure Institute of Pharmaceutical Sciences, Kalaburgi, for providing carried Animal work. Also, the authors are thankful to Medical Scientific Solutions, Hyderabad, for providing chemicals and reagents for this project.

11. References

1. Arcaro G, Koga AY, Carletto B, Budel GM, Gaspar MDd, *et al*. Preclinical trial of *Ocotea puberula* (Rich.) Nees ("*Canela-Guaicá*") in wound healing: Validation of a traditional medicine practice used by indigenous groups in Southern Brazil. Evid Based Complement Alternat Med. 2023; 2023:1-8. https://doi.org/10.1155/2023/3641383 PMid:36818225 PMCid:PMC9935797
2. Taleuzzaman M, Jain P, Verma R, Iqbal Z, Mirza MA. Eugenol as a potential drug candidate: A review. Curr Topic Med Chem. 2021; 21(20):1804-1815. https://doi.org/10.2174/1568026621666210701141433 PMid:34218781
3. Kirubakaran D, Selvam K, Shivakumar MS, Rajkumar M, Kannan S, Navina B. Bio-fabrication of Zinc oxide nanoparticles using Strobilanthes cordifolia: Characterization and evaluation of antioxidant, anti-cholinergic, anti-inflammatory and wound healing activities. ChemistrySelect. 2024; 9(6). https://doi.org/10.1002/slct.202302792
4. Karnwal A, Jassim AY, Mohammed AA, Sharma V, Said M, Sivanesan I. Nanotechnology for healthcare: Plant-derived nanoparticles in disease treatment and regenerative medicine. Pharmaceuticals. 2024; 17(12):1711. https://doi.org/10.3390/ph17121711 PMid:39770553 PMCid:PMC11678348
5. Nagansurkar SB, Yadav HK, Abhay R. Formulation and evaluation of electrospun nanofiber mats of curcumin and leaf extract of *Tinospora cordifolia*: Designed for accelerating diabetic wound healing. Int J Drug Deliv Technol. 2024; 14(02):687-692. https://doi.org/10.25258/ijddt.14.2.12
6. Henrique M, Alexandre, Pontarolo R, Ferreira LM. Status and future scope of soft nanoparticles-based hydrogel in wound healing. Pharmaceutics. 2023; 15(3):874. https://doi.org/10.3390/pharmaceutics15030874 PMid:36986736 PMCid: PMC10057168.
7. Gounden V, Singh M. Hydrogels and wound healing: Current and future prospects. Gels. 2024; 10(1):43. https://doi.org/10.3390/gels10010043 PMid:38247766 PMCid:PMC10815795
8. Wallenwein CM, Weigel V, Hofhaus G, Dhakal N, Schatton W, Gelperina S, *et al*. Pharmaceutical development of nanostructured vesicular hydrogel formulations of rifampicin for wound healing. Int J Mole Sci. 2022; 23(24):16207. https://doi.org/10.3390/ijms232416207 PMid:36555855 PMCid:PMC9788359
9. Jiang Y, Krishnan N, Heo J, Fang RH, Zhang L. Nanoparticle–hydrogel superstructures for biomedical applications. J Cont Rel. 2020; 324:505-521. https://doi.org/10.1016/j.jconrel.2020.05.041 PMid:32464152 PMCid:PMC7429280
10. Gonçalves RC, Signini R, Rosa LM, Dias YSP, Vinaud MC, Lino Junior RdS. Carboxymethyl chitosan hydrogel formulations enhance the healing process in experimental partial-thickness (second-degree) burn wound healing. Acta Cir Bras. 2021; 36(3). https://doi.org/10.1590/acb360303 PMid:33825787 PMCid:PMC8026200
11. Kaur J, Anwer MdK, Sartaj A, Panda BP, Ali A, Zafar A, *et al*. ZnO nanoparticles of *Rubia cordifolia* extract formulation developed and optimized with QbD application, considering *ex vivo* skin permeation, antimicrobial and antioxidant properties. Molecules. 2022; 27(4):1450. https://doi.org/10.3390/molecules27041450 PMid:35209242 PMCid:PMC8878222
12. Daneshmand S, Shiehzadeh F, Mohebi D, Chavoshian O. Formulation, characterization, and optimization of a topical gel containing tranexamic acid to prevent superficial bleeding: *In vivo* and *in vitro* evaluations. Turk J Pharm Sci. 2023; 20(4):261-269. https://doi.org/10.4274/tjps.galenos.2022.60687 PMid:37606011 PMCid:PMC10445226
13. Kumar A, Valamla B, Thakor P, Chary PS, Rajana N, Mehra NK. Development and evaluation of nanocrystals loaded hydrogel for topical application. J Drug Deliv Sci Technol. 2022; 74:103503. https://doi.org/10.1016/j.jddst.2022.103503
14. Weng J, Tong HHY, Chow SF. *In vitro* release study of the polymeric drug nanoparticles: Development and validation

of a Novel method. Pharmaceutics. 2020; 12(8). https://doi.org/10.3390/pharmaceutics12080732 PMid:32759786 PMCid:PMC7465254
15. Nimesh S, Manchanda R, Kumar R, Saxena A, Chaudhary P, Yadav V, *et al*. Preparation, characterization and *in vitro* drug release studies of novel polymeric nanoparticles. Int J Pharm. 2006; 323(1-2):146-52. https://doi.org/10.1016/j.ijpharm.2006.05.065 PMid:16920286
16. Abubakar A, Haque M. Preparation of medicinal plants: Basic extraction and fractionation procedures for experimental purposes. J Pharm Bioall Sci. 2020; 12(1):1-10 https://doi.org/10.4103/jpbs.JPBS_175_19 PMid:32801594 PMCid:PMC7398001
17. Sasidharan S, Chen Y, Saravanan D, Sundram K, Latha L. Extraction, isolation and characterization of bioactive compounds from plants' extracts. Afr J Trad Compl Altern Med. 2010; 8(1). https://doi.org/10.4314/ajtcam.v8i1.60483
18. Bitwell C, Indra SS, Luke C, Kakoma MK. A review of modern and conventional extraction techniques and their applications for extracting phytochemicals from plants. Sci Afr. 2023; 19:1-19. https://doi.org/10.1016/j.sciaf.2023.e01585
19. Bhadange YA, Carpenter J, Saharan VK. A comprehensive review on advanced extraction techniques for retrieving bioactive components from natural sources. ACS Omega. 2024; 9(29):31274-31297. https://doi.org/10.1021/acsomega.4c02718 PMid:39072073 PMCid:PMC11270575
20. Reddy JM, Anitha R, Rajeshkumar S, Lakshmi T. Characterisation of cumin oil mediated silver nanoparticles using UV-visible spectrophotometer and TEM. Res J Pharm Technol. 2019; 12(10):4931. https://doi.org/10.5958/0974-360X.2019.00855.2
21. Mathew S, Prasad AK, Benoy T, Rakesh PP, Hari M, Libish TM, *et al*. UV-visible photoluminescence of TiO_2 nanoparticles prepared by hydrothermal method. J Fluoresc. 2012; 22(6):1563-1569. https://doi.org/10.1007/s10895-012-1096-3 PMid:22763926
22. Liao DL, Wu GS, Liao BQ. Zeta potential of shape-controlled TiO_2 nanoparticles with surfactants. Colloids Surf A: Physicochem Eng Asp. 2009; 348(1-3):270-275. https://doi.org/10.1016/j.colsurfa.2009.07.036
23. Anbuvannan M, Ramesh M, Viruthagiri G, Shanmugam N, Kannadasan N. Synthesis, characterization and photocatalytic activity of ZnO nanoparticles prepared by biological method. Spectrochim. Acta A Mol. Biomol. Spectrosc. 2015; 143:304-308. https://doi.org/10.1016/j.saa.2015.01.124 PMid:25756552
24. Khanna PK, Gaikwad S, Adhyapak PV, Singh N, Marimuthu R. Synthesis and characterization of copper nanoparticles. Mat Lett. 2007; 61(25):4711-4714. https://doi.org/10.1016/j.matlet.2007.03.014
25. Mittal M, Sharma M, Pandey OP. UV–visible light induced photocatalytic studies of Cu doped ZnO nanoparticles prepared by co-precipitation method. Sol Energy. 2014; 110:386-397. https://doi.org/10.1016/j.solener.2014.09.026
26. Bhattacharya S. Central composite design for response surface methodology and its application in pharmacy. Response Surface Methodology in Engineering Science. 2021. https://doi.org/10.5772/intechopen.95835
27. Taleuzzaman M, Sartaj A, Kumar Gupta D, Gilani SJ, Mohd AM. Phytosomal gel of Manjistha Extract (MJE) formulated and optimized with central composite design of Quality by Design (QbD). J Dispersion Sci Technol. 2021; 1-9. https://doi.org/10.1080/01932691.2021.1942036
28. Ahmad N, Bukhari SNA, Hussain MA, Ejaz H, Munir MU, Amjad MW. Nanoparticles incorporated hydrogels for delivery of antimicrobial agents: Developments and trends. RSC Adv. 2024; 14(19):13535-13564. https://doi.org/10.1039/D4RA00631C PMid:38665493 PMCid:PMC11043667
29. Soltani L, Varmira K, Nazari M. Comparison of the differentiation of ovine fetal bone-marrow mesenchymal stem cells towards osteocytes on chitosan/alginate/CuO-NPs and chitosan/alginate/FeO-NPs scaffolds. Sci Rep. 2024; 14(1). https://doi.org/10.1038/s41598-023-50664-6 PMid:38168144 PMCid:PMC10762099
30. Nasir, MAM, Mahammed NL, Roshan S, Ahmed MW.Wound healing activity of poly herbal formulation in albino rats using excision wound model, incision wound model, dead space wound model and burn wound model. Int J Res Dev Pharm L Sci. 2016; 5(2):2080-2087.
31. Yan M, Huang S, Li X, Wang Y, Zhong S, Ban J, *et al*. Gallic acid nanocrystal hydrogel: A novel strategy for promoting wound healing and inhibiting scar formation. Int J Nanomed. 2025; 20:4607-4626. https://doi.org/10.2147/IJN.S514961 PMid:40236519 PMCid:PMC11998940
32. Kłosiński KK, Wach RA, Weronika Kruczkowska, Duda Ł, Kołat D, Żaneta Kałuzińska-Kołat, *et al*. Carboxymethyl chitosan hydrogels for effective wound healing — An animal study. J Funct Biomat. 2023; 14(9):473. https://doi.org/10.3390/jfb14090473 PMid:37754888 PMCid:PMC10531907
33. Jain P, Taleuzzaman M, Kala C, Kumar Gupta D, Ali A, Aslam M. Quality by Design (Qbd) assisted development of phytosomal gel of aloe vera extract for topical delivery. J Liposome Res. 2020; 31(4):381-388. https://doi.org/10.1080/08982104.2020.1849279 PMid:33183121
34. Kalusalingam A, Khan A, Kanakal MM, Abbas SA, Long CM, Tazneem B, *et al*. Enhanced wound healing with *Rhodiola rosea* Phytosomal gel: Extraction, formulation, and *in vivo* evaluation. Curr Pharm Design. 2025; 31. https://doi.org/10.2174/0113816128359150250211053431 PMid:40114578
35. Sarkar T, Bharadwaj KK, Salauddin M, Pati S, Chakraborty R. Phytochemical characterization, antioxidant, anti-inflammatory, anti-diabetic properties, molecular docking,

pharmacokinetic profiling, and network pharmacology analysis of the major phytoconstituents of raw and differently dried *Mangifera indica* (Himsagar cultivar): An *in vitro* and *in silico* investigations. Appl Biochem Biotechnol. 2021; 194(2):950-987. https://doi.org/10.1007/s12010-021-03669-8 PMid:34591254

36. Jeevanandam J, Kiew SF, Boakye-Ansah S, Lau SY, Barhoum A, Danquah MK, *et al*. Green approaches for the synthesis of metal and metal oxide nanoparticles using microbial and plant extracts. Nanoscale. 2022; 14(7):2534-2571. https://doi.org/10.1039/D1NR08144F PMid:35133391
37. Almisbah SRE, Mohammed AMA, Elgamouz A, Bihi A, Kawde A. Green synthesis of CuO nanoparticles using *Hibiscus sabdariffa* L. extract to treat wastewater in Soba Sewage Treatment Plant, Sudan. Water Sci Technol. 2023; 87(12):3059-3071. https://doi.org/10.2166/wst.2023.153 PMid:37387430
38. Nouren S, Bibi I, Kausar A, Sultan M, Bhatti HN, Safa Y, *et al*. Green synthesis of CuO nanoparticles using *Jasmin sambac* extract: Conditions optimization and photocatalytic degradation of Methylene Blue dye. J King Saud Univ - Sci. 2024; 36(3):103089. https://doi.org/10.1016/j.jksus.2024.103089
39. Medjdoub A, Nedjimi MS, Tlili S, Gherab K, Gherissi K. Green synthesis of CuO nanoparticles using aqueous extract of (Artemisia Herba Alba) and their potential applications as antimicrobial agents. Pak J Life Soc Sci. 2024; 22(2). https://doi.org/10.57239/PJLSS-2024-22.2.00161
40. Munandar N, Kasim S, Arfah R, Basir DN, Hala Y, Zakir M, *et al*. Green synthesis of copper oxide (CuO) nanoparticles using *Anredera cordifolia* leaf extract and their antioxidant activity. Comm Sci Technol. 2022; 7(2):127-134. https://doi.org/10.21924/cst.7.2.2022.1004
41. Kumar A, Sofi AH, Hamza B, Rubab S, Shah MA. Eco-friendly synthesis of antibacterial CuO nanoparticles using garlic bulb extract. Green Mat. 2024; 1-10. https://doi.org/10.1680/jgrma.24.00139
42. Bala N. Biogenic fabrication of CuO nanoparticles by *Oxalis corniculata* L. to evaluate antibacterial and hypoglycemic activity on diabetic mice. Int J Pharm Sci Drug Res. 2024; 557-65. https://doi.org/10.25004/IJPSDR.2024.160402
43. Aroob S, Carabineiro SAC, Taj MB, Bibi I, Raheel A, Javed T, *et al*. Green synthesis and photocatalytic dye degradation activity of CuO nanoparticles. Catalysts. 2023; 13(3):502. https://doi.org/10.3390/catal13030502
44. Alizadeh S, Samadikuchaksaraei A, Jafari D, Orive G, Dolatshahi-Pirouz A, Pezeshki-Modaress M, *et al*. Enhancing diabetic wound healing through improved angiogenesis: The role of emulsion-based core-shell micro/nanofibrous scaffold with sustained CuO nanoparticle delivery. Small. 2024; 20(24):e2309164. https://doi.org/10.1002/smll.202309164 PMid:38175832

Author Contribution

Rakesh Surappa Anjaneya and Guno Sindhu Chakraborty: Conception, design, writing manuscript, resources, literature search, data collection, and critical review, both authors equally contributed. All authors have read and agreed to the published version of the manuscript.